

Therefore, it is meaningless to say that $d\sigma/dt$ has kinematic t singularities, unless we specify that B^t be used in the expression of $d\sigma/dt$.

From the above discussion, it is clear that if $t=0$ is approachable by experiment, then $B^t(=B^s)$ should be finite at $t=0$. We are interested in the situation where the point $t=0$ cannot be approached by experiment but is very near the physical region. Let us now investigate the case $M_a=M_c$, $M_b \neq M_d$. In this case, we have $\cos\theta_t=0$ at $t=0$, i.e., both $\cos(\theta_t/2)$ and $\sin(\theta_t/2)$ are finite at $t=0$. From the expression

$$B^t(s,t) = \sum_{c,A,D,b} |\bar{f}_{cA,D}^t(s,t) (\cos\frac{1}{2}\theta_t)^{|\lambda'+\mu'|} \times (\sin\frac{1}{2}\theta_t)^{|\lambda'-\mu'|} |^2,$$

we see that the behavior of B^t near the point $t=0$ is determined only by \bar{f}^t which are related to \bar{f}^s by the Trueman-Wick crossing relation. Since \bar{f}^s do not have kinematic t singularities, only the coefficients $M_{cd,ab}^{c'A',D'b'}$ (s,t) have to be checked. At $t=0$, these

coefficients diverge if and only if one of the $\cos\chi$'s diverges. (The same χ 's appear in both $M_{cd,ab}^{c'A',D'b'}$ and $M_{c'A',D'b',cd,ab}$.) Two of the $\cos\chi$'s behave like $t^{-1/2}$, while others are finite as $t \rightarrow 0$. However, in the physical region, all of them satisfy the restriction $|\cos\chi| \leq 1$. In other words, χ 's are defined to be real angles in the physical region; therefore, no matter how small t is in the physical region, the functions $\cos\chi$ and f^t are not dominated by the kinematic singularities at $t=0$. Thus, we conclude that the kinematic singularities of the t -channel helicity amplitudes at $t=0$ can be ignored in any phenomenological analysis of the two-particle reaction.

ACKNOWLEDGMENTS

The author would like to thank Dr. Fei-Shian Chen Cheung for drawing his attention to this interesting question, and Professor P. Carruthers for helpful discussion.

Reaction $K^-p \rightarrow \Lambda\omega$ from 1.2 to 2.7 BeV/c: The Absorption Model with Strange-Meson Exchange*

STANLEY M. FLATTÉ

Lawrence Radiation Laboratory, University of California, Berkeley, California

(Received 5 October 1966)

We have analyzed over 9000 $K^-p \rightarrow \Lambda\omega \rightarrow (p\pi^-)(\pi^+\pi^-\pi^0)$ events in four momentum regions between 1.2 and 2.7 BeV/c. We have systematically determined the differential cross section and the 11 independent decay-correlation parameters as a function of production angle for each of the four momentum regions. A striking forward peak in the differential cross section at our highest momentum, 2.6 BeV/c, suggests the appearance of strange-meson exchange. Using a new formalism for the absorption model, we show that the behavior of the differential cross section and the decay-correlation parameters at 2.6 BeV/c as a function of production angle is qualitatively explained by the absorption model with K and K^* exchange. Using available data on $K^-p \rightarrow \Lambda\phi$ at 2.6 BeV/c, we show that the absorption model also explains the behavior of $K^-p \rightarrow \Lambda\phi$, and that the comparison between the couplings of $K^-p \rightarrow \Lambda\omega$ and $K^-p \rightarrow \Lambda\phi$ is in reasonable agreement with $SU(3)$ predictions.

I. INTRODUCTION

A. Historical Note

IN quantum electrodynamics both photons and charged particles provide the forces of interaction; in strong interactions, therefore, it is thought that the forces are created by the exchange of mesons and baryons, the known strongly interacting particles.

The attempt to put this philosophy into practice has led physicists down many paths; simple field theory, a direct translation from quantum electrodynamics; S -matrix theory and bootstrap dynamics,¹ based on the

analyticity requirements of amplitudes; Regge poles,² involving analytic continuation in angular momentum variables; and lately, the absorption model,³ a more specialized approach with limited application. In all these approaches, exchanges may take place in either the direct channel (resonances) or in crossed channels (meson or baryon exchanges). The absorption model, which is our concern in the body of this paper, deals most successfully with meson exchanges.

The absorption model has its motivation in the simple Feynman diagram of Fig. 1(a). The basic contribution of the model is the addition of the diagrams of Fig. 1(b)

* This work was done under a fellowship grant from the National Science Foundation and under the auspices of the U. S. Atomic Energy Commission.

¹ See, for example, M. Jacob and G. F. Chew, *Strong Interaction Physics* (W. A. Benjamin, Inc., New York, 1964).

² See, for example, S. C. Frautchi, *Regge Poles and S-Matrix Theory* (W. A. Benjamin, Inc., New York, 1963).

³ See, for example, J. D. Jackson, *Rev. Mod. Phys.* **37**, 484 (1965).

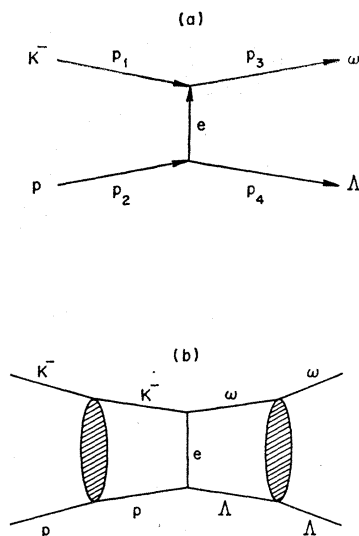


FIG. 1. (a) Diagram for $K^-p \rightarrow \Lambda\omega$ representing one-particle exchange. We consider particle e as being a \bar{K} or K^* meson. (b) Diagram used in the absorption-model calculations. The shaded blobs represent elastic scattering.

involving elastic scattering in the initial and final state. Although the foregoing explanation appears to put the absorption model squarely under field theory, Ball and Frazer⁴ have used S -matrix language to justify

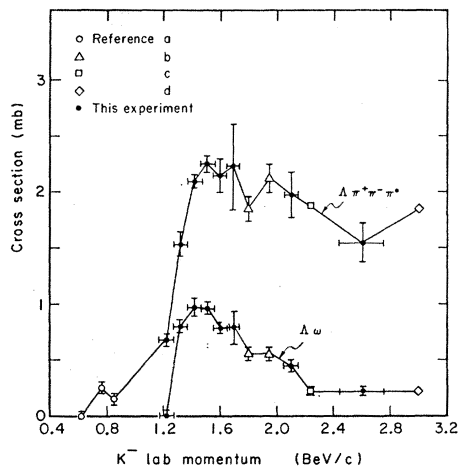


FIG. 2. Cross sections of the reactions (top curve) $K^-p \rightarrow \Lambda\pi^+\pi^- \times \pi^0$ and (bottom curve) $K^-p \rightarrow \Lambda + (\omega \rightarrow \pi^+\pi^-\pi^0)$ from threshold to 3 BeV/c incident- K^- momentum. The connecting lines are only to eliminate confusion. (a) P. L. Bastien and J. P. Berge, Phys. Rev. Letters **10**, 188 (1963). (b) P. M. Dauber, W. M. Dunwoodie, P. E. Schlein, W. E. Slater, L. T. Smith, D. H. Stork, and H. K. Ticho, in Proceedings of the Second Topical Conference on Resonant Particles, Athens, Ohio, 1965 (unpublished); L. T. Smith, Ph.D. thesis, University of California, Los Angeles (unpublished). (c) P. L. Connolly, E. L. Hart, K. W. Lai, G. C. Moneti, R. R. Rau, N. P. Samios, I. O. Skillicorn, S. S. Yamamoto, M. Goldberg, M. Gundzik, J. Leitner, and S. Lichtman, in *Proceedings of the Sienna International Conference on Elementary Particles* (Societa Italiana di Fisica, Bologna, 1963), p. 130. (d) E. S. Gelsema, J. C. Kluyver, A. G. Tenner, M. Demoulin, J. Goldberg, B. P. Gregory, G. Kayas, P. Krejbich, C. Pelletier, R. Barloutand, A. Leveque, C. Louedec, J. Meyer, and A. Verglas, in *Proceedings of the Sienna International Conference on Elementary Particles* (Societa Italiana di Fisica, Bologna, 1963), p. 134.

⁴ J. S. Ball and W. R. Frazer, Phys. Rev. Letters **14**, 746 (1965).

the basic equations of the model, at least for pseudo-scalar exchange. The model has been applied with reasonable success⁵ to $\pi^-p \rightarrow \rho^-p$, $Kp \rightarrow K^*p$, and many other reactions involving pion and nonstrange vector-meson exchange, as well as $K^-p \rightarrow \pi^-Y_1^*$, involving K^* exchange.⁵ Here we apply the absorption model to $K^-p \rightarrow \Lambda\omega$ and $K^-p \rightarrow \Lambda\phi$, which involve K and K^* exchange.

B. Summary of Results

We have analyzed over 9000 $K^-p \rightarrow \Lambda\omega \rightarrow (p\pi^-)$ ($\pi^+\pi^-\pi^0$) events in four momentum regions between 1.2 and 2.7 BeV/c. We have systematically determined the differential cross section and the eleven decay-correlation parameters as a function of production angle for each of the four momentum regions. In this section of the Introduction, we will indicate our line of thinking as to the implications of our results.

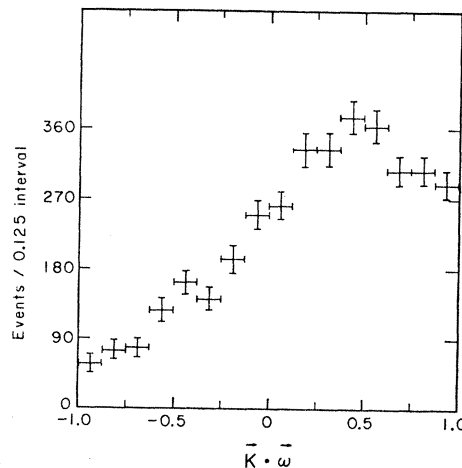


FIG. 3. Production-angle distribution for $K^-p \rightarrow \Lambda\omega$ at 1.5 BeV/c; background has been subtracted, leaving 3570 events.

Figure 2 shows the total cross section for $K^-p \rightarrow \Lambda\omega$ as a function of beam momentum. We note that there are no striking resonance phenomena; the cross section rises from threshold and falls smoothly in the usual manner for inelastic reactions, at least within our statistics. There is a known resonance, $Y_0^*(2100)$, with correct quantum numbers for decay into $\Lambda\omega$. A laboratory K^- momentum of 1.7 BeV/c corresponds to a center-of-mass energy of 2100 MeV. We can set an upper limit for the branching ratio into $\Lambda\omega$:

$$\frac{Y_0^*(2100) \rightarrow \Lambda\omega}{Y_0^*(2100) \rightarrow \text{all}} < 0.1.$$

Now it is perfectly possible that there are other resonances in this region, and it is even possible that an extremely careful analysis of the data could give some

⁵ J. D. Jackson, J. T. Donohue, K. Gottfried, R. Keyser, and B. E. Y. Svensson, Phys. Rev. **139**, B428 (1965).

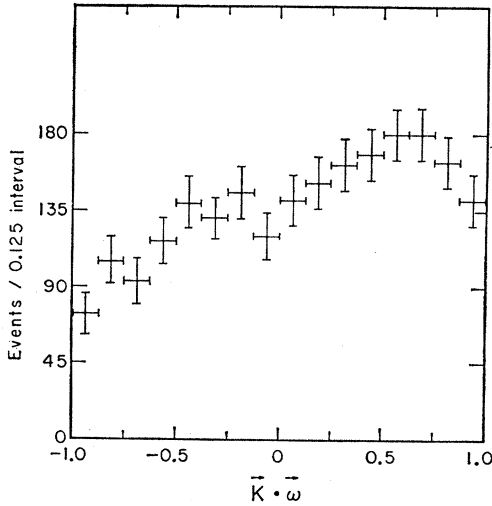


FIG. 4. Production-angle distribution for $K^-p \rightarrow \Lambda\omega$ at 1.7 BeV/c; background has been subtracted, leaving 1570 events.

indications of them, but the separation of the data into smaller energy intervals would reduce the accuracy of the measurements, because of poor statistics, to such an extent that conclusions could be drawn only with difficulty.

If we focus our attention on the production-angle distributions, Figs. 3 through 6, we see that only very low partial waves are needed to explain the 1.5-, 1.7-, and 2.1-BeV/c data, but a very striking forward peak appears at 2.6 BeV/c. This peak could be caused by the interference of high partial-wave amplitudes coming from some direct-channel activity [see Fig. 7(a)]; we prefer to interpret it as most forward peaks in interactions around this energy have been interpreted—as the effect of poles in the crossed channel [see Fig. 7(b)]; in our case, strange-meson exchange.

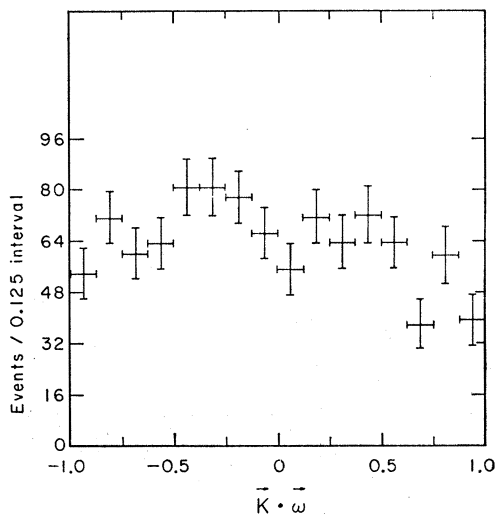


FIG. 5. Production-angle distribution for $K^-p \rightarrow \Lambda\omega$ at 2.1 BeV/c; background has been subtracted, leaving 1021 events.

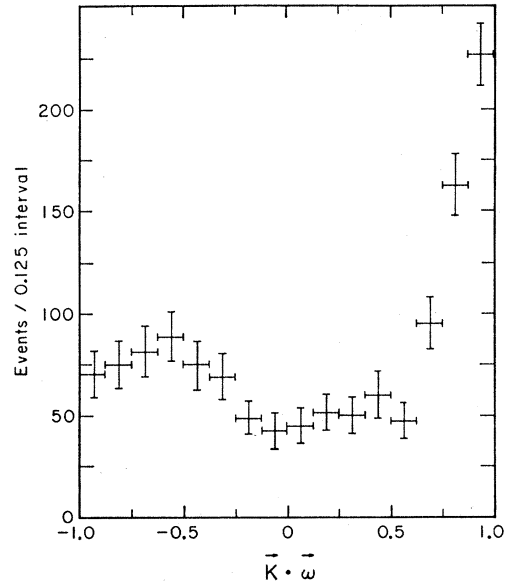


FIG. 6. Production-angle distribution for $K^-p \rightarrow \Lambda\omega$ at 2.6 BeV/c; background has been subtracted, leaving 1300 events.

A broad peak in the differential cross section also appears near the backward direction at 2.6 BeV/c (Fig. 6). Fried and Taylor have interpreted similar data at 3 BeV/c as a manifestation of nucleon exchange.⁶ While this explanation is possible, the smooth variation of the production-angle distribution from 1.5 through 2.1 BeV/c makes it seem similarly plausible that the hump at 2.6 BeV/c (and, presumably, the one at 3 BeV/c) is simply a continuation of low partial-wave behavior associated with threshold and resonance effects.

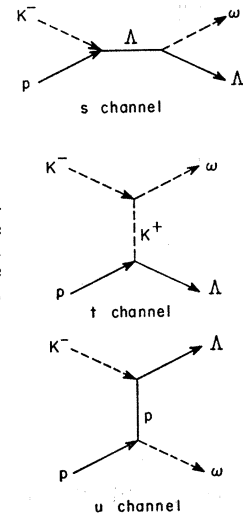


FIG. 7. Feynman diagrams representing exchanges in the three channels that affect $K^-p \rightarrow \Lambda\omega$. Exchanges of the least massive particles are shown. (a) s channel, (b) t channel, (c) u channel.

⁶H. M. Fried and J. G. Taylor, Phys. Rev. Letters **15**, 709 (1966). See also H. Sugawara and F. von Hippel, Phys. Rev. **145**, 1331 (1966).

Hence we systematically present our data at all momenta, believing that the data represent the effects of threshold and perhaps some resonance behavior, except for the striking forward peak at 2.6 BeV/c, which we associate with strange-meson exchange.

Before we consider the absorption model, we should discuss why we did not apply any Regge-pole analysis to our data. Briefly, our data are at too low an energy. The requirement that a Regge-pole approximation be valid is usually expressed in terms of $\cos\theta_t$, where θ_t is the "production angle" in the crossed channel. Since θ_t is an unphysical angle, $|\cos\theta_t|$ is greater than 1; the validity criterion is $|\cos\theta_t| \gg 1$. (At least, plead the advocates of Regge poles, have $|\cos\theta_t| \gtrsim 5$.) At 1.5 BeV/c in $K^-p \rightarrow \Lambda\omega$, we have $|\cos\theta_t|$ between 1.0 and 1.5; at 2.6 BeV/c, we almost, but not quite, reach $|\cos\theta_t|=3$. Hence it would have very little meaning to apply Regge poles at our energies. It is the absorption model that has had success at these energies.

We use a new formalism for the absorption model developed by Huff,⁷ in which a linear-momentum representation is used instead of the usual angular-momentum representation involving partial-wave decomposition. We show that:

1. The absorption model has excellent success in fitting the differential cross section and qualitative success in fitting the decay parameters of $K^-p \rightarrow \Lambda\omega$ at 2.6 BeV/c in the forward direction.

2. Where it is not applicable, namely the lower momentum regions, the absorption model fails to give reasonable fits.

3. The K -meson-exchange coupling determined in an unconstrained variation of parameters is in remarkable agreement with the $SU(3)$ prediction, and the K^* -exchange couplings are of a reasonable order of magnitude.

4. The reaction $K^-p \rightarrow \Lambda\phi$ at 2.6 BeV/c in the

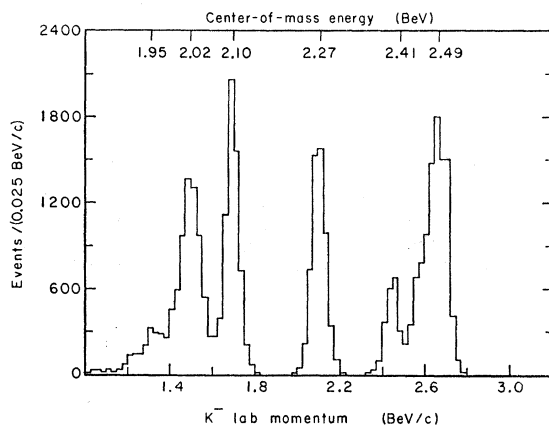


FIG. 8. Distribution of beam momentum for 31 800 events of the type $K^-p \rightarrow \Lambda\pi^+\pi^-\pi^0$. Over one million pictures were taken to gather this data.

⁷ Robert W. Huff, Physics Department, University of California at Los Angeles, 1965 (private communication).

forward direction is also reasonably well explained by the absorption model, and the comparison of the K - and K^* -exchange couplings determined for $K^-p \rightarrow \Lambda\phi$ with those determined for $K^-p \rightarrow \Lambda\omega$ is in agreement with $SU(3)$.

II. ANALYSIS OF THE DATA

A. Introduction

Approximately 9400 events of the reaction $K^-p \rightarrow \Lambda\omega \rightarrow (p\pi^-)\pi^+\pi^-\pi^0$ have been identified in a K^- exposure of the 72-in. hydrogen bubble chamber. The momentum settings ranged from 1.2 to 2.7 BeV/c. Figure 8 shows the beam-momentum spectrum for 32 000 events of the type $K^-p \rightarrow \Lambda\pi^+\pi^-\pi^0$. Since the cross section for the reaction $K^-p \rightarrow \Lambda\pi^+\pi^-\pi^0$ is changing in this energy region, Fig. 8 does not reflect the relative amount of film taken at the various momenta. Table I summarizes the data taken at each momentum setting in terms of the number of events per millibarn of cross section.

The bubble chamber was exposed in two different runs, with the use of two entirely different beam configurations.^{8,9} The method for identifying the desired events in the first run, designated K72 and with beam momenta from 1.2 to 1.7 BeV/c, has already been given in a previous publication.¹⁰ The analysis of the second run, designated K63 and with beam momenta from 1.7 to 2.7 BeV/c, is given in detail here. For the reader's convenience we include the important parameters of the first run where they are of interest.

B. Scanning and Measuring

The film was scanned once and the events found were measured. All V +two-prong events were fit to the following hypotheses:

$$K^-p \rightarrow \Lambda\pi^+\pi^- \quad (1)$$

$$\Lambda\pi^+\pi^-\pi^0 \quad (2)$$

$$\Lambda K^+K^- \quad (3)$$

$$\Sigma^0\pi^+\pi^- \quad (4)$$

$$\Sigma^0 K^+K^- \quad (5)$$

$$p\pi^-\bar{K}^0 \quad (6)$$

$$p\pi^-\pi^0\bar{K}^0 \quad (7)$$

$$n\pi^+\pi^-\bar{K}^0, \quad (8)$$

⁸ J. J. Murray, J. Button-Shafer, F. T. Shively, G. H. Trilling, J. A. Kadyk, A. Rittenberg, D. M. Siegel, J. A. Lindsey, and D. W. Merrill, in *Proceedings of the International Conference on High-Energy Physics Dubna, 1964* (Atomizdat, Moscow, 1966), Vol. II, p. 541. See also D. Merrill, Alvarez Physics Note No. 519, 1964 (unpublished); S. Flatté, S. Chung, L. Hardy, and R. Hess, Alvarez Physics Note No. 524, 1964 (unpublished).

⁹ See, for example, Charles G. Wohl, University of California Lawrence Radiation Laboratory Report No. UCRL-16288, 1965 (unpublished).

¹⁰ S. M. Flatté, D. O. Huwe, J. J. Murray, J. Button-Shafer, F. T. Solmitz, M. L. Stevenson, and C. G. Wohl, *Phys. Rev.* **145**, 1050 (1966).

TABLE I. Total cross sections for $K^-p \rightarrow \Lambda\omega \rightarrow \Lambda\pi^+\pi^-\pi^0$.

Run	Momentum (BeV/c)	Path length (events/ μ b)	$\sigma_{\Lambda\pi^+}$ ^a (mb)	$N(3\pi)$	$N(\omega)$	$\sigma_{\Lambda\omega}$ ^a (mb)
K72	1.22	1.23 \pm 0.06	0.68 \pm 0.05	392	0 \pm 30	0 \pm 0.05
	1.32	1.44 \pm 0.07	1.53 \pm 0.10	965	502	0.80 \pm 0.06
	1.42	0.83 \pm 0.04	2.10 \pm 0.06	1093	505	0.97 \pm 0.08
	1.51	5.09 \pm 0.20	2.26 \pm 0.08	5847	2475	0.96 \pm 0.05
	1.60	0.72 \pm 0.04	2.14 \pm 0.15	1006	366	0.78 \pm 0.05
	1.70	1.10 \pm 0.06	2.82 \pm 0.17	1000	357	1.01 \pm 0.06
K63	1.7	3.86 \pm 0.20 ^b	1.66 \pm 0.25	2923	1060	0.58 \pm 0.10
	2.1	6.04 \pm 0.30 ^b	1.98 \pm 0.20	5563	1299	0.46 \pm 0.05
	2.6	16.5 \pm 0.9 ^b	1.55 \pm 0.16	11 831	1660	0.22 \pm 0.03

^a Corrected for neutral Λ decay.^b For 2.1 and 2.6 BeV/c, path lengths were obtained from Lindsey (Ref. 30). At 1.7 BeV/c we used the same method of counting τ s as he did.

where the Σ^0 always decays into $\Lambda\gamma$, Λ decays into $p\pi^-$, and \bar{K}^0 decays into $\pi^+\pi^-$.

V +two-prongs are fitted to hypotheses (1) through (8) in two steps. First, the neutral V direction is taken to be the line connecting the primary vertex to the vertex of the V , and the V is fit to two hypotheses, $\Lambda \rightarrow p\pi^-$ and $\bar{K}^0 \rightarrow \pi^+\pi^-$. These are three-constraint fits. For $\chi^2(\Lambda) < 32$, reaction hypotheses (1) through (5) are tried; for $\chi^2(\bar{K}^0) < 32$, reaction hypotheses (6) through (8) are tried. For $\chi^2(\Lambda)$ and $\chi^2(\bar{K}^0)$ each less than 32, all production hypotheses are tried; in this case if an acceptable χ^2 is obtained from some production process for both interpretations of the V , the event is classified as ambiguous between Λ and \bar{K}^0 production. The percentage of ambiguous events varied from 2.2% at 1.7 BeV/c to 6.7% at 2.6 BeV/c. (In K72 the percentage varied from 1.2% at 1.2 BeV/c to 2.5% at 1.7 BeV/c. The two independently analyzed samples at 1.7 BeV/c thus agree.) Most of the ambiguous events are Λ events.¹⁰

We must now consider how to separate type-2 events from those of types 1, 3, 4, 5, and 6. Events that simultaneously fit reactions (2) and (1) or (3) constitute less than 2% of the sample which fits (2). Consequently the $\Lambda\pi^+\pi^-\pi^0$ events are free from contamination by $\Lambda\pi^+\pi^-$ or ΛK^+K^- events. The task of separating the other reactions is not so simple. Since the γ ray and the Λ of (4) and (5) are constrained to have the Σ^0 mass, reactions (4) and (5) are two-constraint fits, while reaction (2) is a one-constraint fit. If our measurement errors were properly estimated and were free from systematic errors, the mean value of χ^2 (production), for events that are truly of the type being fitted, would be equal to the number of the constraint class. Actually our errors are underestimated, so that this equality does not hold in general. Nevertheless, a confidence level is calculated for each hypothesis. Events are accepted as being a particular reaction if the confidence level for that reaction is greater than the confidence levels of all other hypotheses and the confidence level is greater than 0.005. If all confidence levels are less than 0.005, the event is classified as a failure.

The failing rate for first measurements is not small

(between 30 and 40%) and therefore events that have failed are measured a second time, and sometimes even a third time. Both second and third measurements have about a 50% failing rate.

C. Scanning and Measuring Biases

We must now consider the possibility that the loss of events due to scanning and measuring errors has biased the angular distributions in which we are interested.

1. Scanning Biases

We have checked for two possible scanning biases.

a. Opening angle of the Λ . The direction of the pion in the Λ rest frame makes an angle ψ with respect to the direction of the Λ in the laboratory. (The Λ laboratory direction remains the same when transformed to the Λ rest frame.) If the scanning contains no biases against certain opening angles, then the distribution of $\cos\psi$ should be flat. Figure 9 illustrates the distribution of $\cos\psi$ for 1.7 BeV/c. The other momenta have similarly flat distributions.

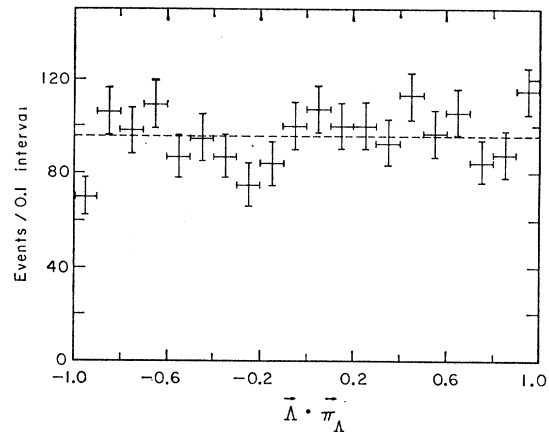


FIG. 9. Distribution of $\cos\psi = \mathbf{\Lambda} \cdot \boldsymbol{\pi}$ in the Λ rest frame, where $\mathbf{\Lambda}$ is the direction of the Λ in the laboratory. This graph, for $K^-p \rightarrow \Lambda\pi^+\pi^-\pi^0$ events at 1.7 BeV/c in the ω region, exhibits no bias against any opening angle for the Λ .

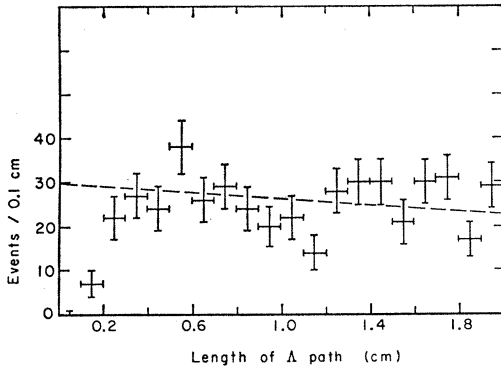


FIG. 10. Distribution of length of the Λ path for $K^-p \rightarrow \Lambda\pi^+\pi^-\pi^0$ events at 1.7 BeV/c in the ω region, showing a loss of events at small lengths due to scanning bias. The dashed curve is the expected exponential if all Λ 's had a laboratory momentum of 1 BeV/c, which is about the average in this sample.

b. Λ -length cutoff. An event in which the Λ has decayed within a few millimeters of the production vertex is difficult to distinguish from a four-prong event. The distribution of the length of the Λ , shown in Fig. 10 for 1.7 BeV/c, deviates from the expected approximate exponential at 2 or 3 mm and less. To check whether this causes a bias in angular distributions for $K^-p \rightarrow \Lambda\omega$ we have compared the center-of-mass (c.m.) production-angle distribution for events with $750 \text{ MeV} < M(\pi^+\pi^-\pi^0) < 810 \text{ MeV}$ at 2.6 BeV/c with a production-angle distribution obtained from the same events in the following way: All events whose Λ went less than 2 mm in the laboratory were discarded, and each remaining event was weighted by the factor $\exp[x/\eta c\tau]$, where x is the Λ -length cutoff (2 mm), η is the laboratory momentum of the Λ in BeV/c divided by the mass of the Λ in BeV/c², and τ is the mean life of the Λ . It should be noted that at 2.6 BeV/c and below, the Λ is constrained to the forward 45-deg cone in the

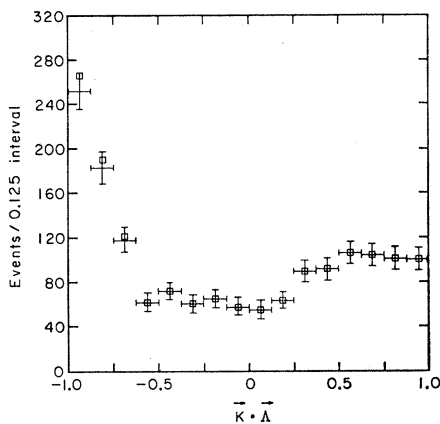


FIG. 11. Production-angle distributions for $K^-p \rightarrow \Lambda\pi^+\pi^-\pi^0$ events at 2.6 BeV/c with $750 \text{ MeV} < M(\pi^+\pi^-\pi^0) < 810 \text{ MeV}$. The boxes indicate points we obtained by imposing a 2-mm cutoff on the Λ laboratory length and appropriately weighting the remaining events.

laboratory. We have chosen 2.6 BeV/c as our sample because two reasons indicate that the bias should be worst at the highest momentum; first, the Λ can go slowest in the laboratory, and second, the correction is largest for Λ 's that go backwards in the center of mass and the 2.6-BeV/c production-angle distribution is sharply peaked in the backward direction (forward direction for the three-pion system). Figure 11 shows the unweighted distribution with the weighted points shown as boxes. The corrections are within the error bars, and it should be remembered that when background is subtracted, the estimated errors will increase. Since the decay correlations will be much less affected by this bias than the production-angle distributions, we have not weighted events in any of our analyses of angular distributions.

No scanning biases relating to the two prongs in the V +two-prong events have been discovered.

2. Measuring Biases

Possible measuring biases due to the large failure rates in first and second measurements have been investigated in the following way: Angular distributions for events which passed the first measurement are compared with those that failed the first measurement but passed the second. Figure 12 shows the production-angle distributions for two such samples. No significant differences are noted. Twice-failing events have been scanned and no obvious biases were detected.

D. Ambiguities

Among the 6300 events in the K63 run which fit $K^-p \rightarrow \Lambda\pi^+\pi^-\pi^0$ and have a $M(\pi^+\pi^-\pi^0)$ in the ω region, there are undoubtedly a small number of events that are really of other reaction types. However, there is no reason to suppose that these events create a peak in the mass spectrum near the ω mass, which might be confused with the ω . Since ambiguities are known to constitute less than 10% of the $\Lambda\pi^+\pi^-\pi^0$ sample, the contamination of other reactions in the ω region is less than 10% of background, and therefore is negligible. (Of course, we believe that the contamination from other

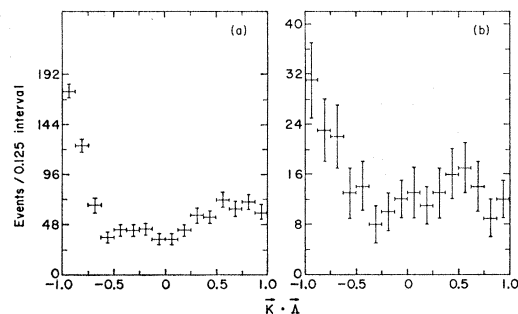


FIG. 12. Production-angle distributions for $K^-p \rightarrow \Lambda\omega$ events at 2.6 BeV/c in the ω region which (a) passed first measurement, and (b) failed first measurement but passed second measurement.

TABLE II. Scanning and measuring correction factors for total-cross-section determinations of V +two-prong events.

	Momentum (BeV/c)		
	1.7	2.1	2.6
Events on first scan	17 988	28 326	71 722
Scanning efficiency (%)	94±3	97±3	94±3
Scanning correction factor ^a	1.10±0.04	1.08±0.04	1.14±0.04
Events not measured	1682	1064	5848
Events measured at least once	16 306	27 262	65 874
Events passing first measurement	10 652	19 266	38 420
First-measurement passing fraction (%)	65	71	58
Events measured at least twice	3745	0	14 877
Events passing second measurement	1720	0	7040
Second-measurement passing fraction (%)	46	47 ^b	47
Events measured at least thrice	0	0	2896
Events passing third measurement	0	0	1448
Third-measurement passing fraction	50 ^b	50 ^b	50
Total passing events	12 372	19 266	46 908
Projected passing events	15 500	25 300	59 800
Measuring correction factor	1.26±0.04	1.31±0.04	1.28±0.04

^a Includes corrections for short Λ and escaping Λ .

^b Where no information is available, the passing fraction of 2.6 BeV/c is used.

reactions is much less than this 10% ambiguity percentage because we think we have estimated confidence levels reasonably well. The upper limit considered here is nevertheless satisfying.) We have further reduced the effect of any background by the subtraction technique outlined in Sec. III.

E. Total-Cross-Section Determinations

Total cross sections in the K72 run have been published.¹¹ The values are listed in Table I.

In the K63 experiment, total K^- path lengths have been determined by Lindsey and Smith¹² at all momenta except 1.7 BeV/c. We determined the path length at 1.7 BeV/c by counting τ decays of the K^- in the same manner as they.

If we divide the total number of good events in a certain fiducial volume that come through the system at a particular momentum setting by the path length at that momentum we will obtain a total cross section for the reaction we are studying. The number we obtain, however, needs several corrections.

1. Scanning Inefficiency

We obtained the scanning efficiencies by scanning the film a second time and comparing the list of events found with the list of good events whose Λ has a length greater than 5 mm. (We correct for Λ length cutoff separately, and we would not want to do it twice.) Good events are those that were found on the first scan and that fit the hypothesis $K^-p \rightarrow \Lambda\pi^+\pi^-\pi^0$. Then the scanning efficiency is (number of good events found on the second scan)/(number of good events). The scanning efficiencies varied from 94 to 97%. (In K72, the scanning efficiencies varied from 94 to 98%.) Table II lists scanning efficiencies.

¹¹ P. Eberhard, S. M. Flatté, D. O. Huwe, J. Button-Shafer, F. T. Solmitz, and M. L. Stevenson, Phys. Rev. **145**, 1062 (1962).

¹² J. A. Lindsey and G. A. Smith, Phys. Rev. **147**, 913 (1966).

2. Measuring Inefficiency

We calculated an effective measuring efficiency by computing passing rates (number passed/number measured) for first, second, and third measurements, and using these numbers to project the failing and unmeasured events through third measurement. Of 120 000 V +two-prong events in K63, 79 000 have passing measurements, and 21 000 more would pass if we completed the measuring program through third measurements. It might appear that 20 000 events are unaccounted for. However, twice-failing events were scanned, and it was discovered that about 50% of them were not V +two-prong events. Projections show that 23 000 events should fail twice and thus we know that in our sample about 12 000 events are not V +two-prong events. We have therefore accounted for all the V +two-prong events to within 6%.

Table II lists correction factors that must be used to multiply the number of passing events to obtain the true number of events of a particular reaction.

3. Λ Length Cutoff

The distribution in proper time (length/momentum) for the Λ 's in our sample, which we expect to be an exponential with decay corresponding to the mean life of the Λ , is seen to drop in the region of short times. We account for the missing events at both ends of the time spectrum, and find corrections of 4±3% at 1.7 BeV/c, 5±3% at 2.1 BeV/c and 5±3% at 2.6 BeV/c.

4. Dalitz Decay of the π^0

The π^0 from ω decay will give a Dalitz pair at the production vertex 1.25% of the time. The event would then be a V +four-prong event and hence would be lost to our V +two-prong sample. We must increase each cross section by 1.25% to account for this effect.

Total cross sections are given in Table I and in Fig. 2.

After considerable analysis we have obtained an unbiased group of events of the type $K^-p \rightarrow \Lambda\omega \rightarrow \Lambda\pi^+\pi^-\pi^0$, and the normalization needed to obtain total cross sections is well understood.

III. RESULTS OF THE ANALYSIS

A. Introduction

We are considering $K^-p \rightarrow \Lambda\omega$ events in which the ω decays into $\pi^+\pi^-\pi^0$ and the Λ decays into $p\pi^-$. There is an extremely large amount of data contained in every event of this type; our problem is to present the data in a useful and understandable form.

First we define the variables (vectors, such as the decay pion momentum from the Λ ; and scalars, such as the c.m. energy) which characterize each event and which can vary from event to event. The differential cross section can then be expressed as a function of these variables in a simple way. The parameters of this function express concisely our knowledge of the reaction. (For example, one may express the knowledge of an angular distribution by giving only the coefficients of the Legendre polynomials in the expression for the angular distribution.)

B. Definition of Internal Variables

In the c.m. system, illustrated in Fig. 13, we use as variables the c.m. energy E and the production angle θ , defined by

$$\cos\theta = \mathbf{K} \cdot \boldsymbol{\omega} / |\mathbf{K}| |\boldsymbol{\omega}|.$$

We obtain all rest-frame quantities by first transforming to the center-of-mass system and then to the rest frame in question. Unit vectors defined in the ω rest frame are:

\mathbf{n} = normal to the plane of the pions from the ω decay ($\boldsymbol{\pi}^- \times \boldsymbol{\pi}^+$).

\mathbf{N} = normal to the production plane $\mathbf{K} \times \boldsymbol{\omega}$ (defined in the c.m. frame and unchanged when shifted to the ω rest frame).

\mathbf{X} , \mathbf{Y} , and \mathbf{N} = an orthogonal set of axes defined by the production process (e.g., \mathbf{K} , $\mathbf{N} \times \mathbf{K}$, \mathbf{N}).

Unit vectors defined in the Λ rest frame are:

$\boldsymbol{\pi}$ = direction of the pion from the Λ decay.

\mathbf{N} = normal to the production plane (same as in ω rest frame).

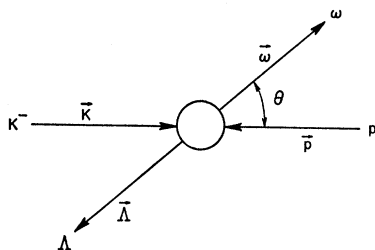


FIG. 13. Schematic drawing of a $K^-p \rightarrow \Lambda\omega$ reaction indicating momentum vectors and the production angle θ in the c.m. system.

\mathbf{X}' , \mathbf{Y}' , and \mathbf{N} = an orthogonal set of axes defined by the production process (e.g., \mathbf{p} , $\mathbf{N} \times \mathbf{p}$, \mathbf{N}).

C. Expressions for Cross Sections

Byers and Yang¹³ and Berman and Oakes¹⁴ have exhibited the general dependence of this reaction on the angles formed in the decays of the final-state particles, given an unpolarized target. Huff¹⁵ has also discussed this reaction. Ademollo and Gatto¹⁶ treated the production characteristics of reactions of this type by means of a density-matrix formalism; such a treatment is the connecting link between the correlations in this section and the production amplitudes. Of course, the spins and parities of the ω and Λ are taken to be 1^- and $\frac{1}{2}^+$, respectively. We may express the entire dependence of the cross section on internal variables as

$$\begin{aligned} d^5\sigma = & [F_1(\mathbf{n} \cdot \mathbf{N})^2 + F_2(\mathbf{n} \cdot \mathbf{X})^2 + F_3(\mathbf{n} \cdot \mathbf{Y})^2 + F_4(\mathbf{n} \cdot \mathbf{X})(\mathbf{n} \cdot \mathbf{Y}) \\ & + F_5(\mathbf{n} \cdot \mathbf{N})^2(\boldsymbol{\pi} \cdot \mathbf{N}) + F_6(\mathbf{n} \cdot \mathbf{X})^2(\boldsymbol{\pi} \cdot \mathbf{N}) + F_7(\mathbf{n} \cdot \mathbf{Y})^2 \\ & \times (\boldsymbol{\pi} \cdot \mathbf{N}) + F_8(\mathbf{n} \cdot \mathbf{X})(\mathbf{n} \cdot \mathbf{Y})(\boldsymbol{\pi} \cdot \mathbf{N}) + F_9(\mathbf{n} \cdot \mathbf{N}) \\ & \times (\mathbf{n} \cdot \mathbf{X})(\boldsymbol{\pi} \cdot \mathbf{X}') + F_{10}(\mathbf{n} \cdot \mathbf{N})(\mathbf{n} \cdot \mathbf{Y})(\boldsymbol{\pi} \cdot \mathbf{X}') \\ & + F_{11}(\mathbf{n} \cdot \mathbf{N})(\mathbf{n} \cdot \mathbf{X})(\boldsymbol{\pi} \cdot \mathbf{Y}') + F_{12}(\mathbf{n} \cdot \mathbf{N})(\mathbf{n} \cdot \mathbf{Y})(\boldsymbol{\pi} \cdot \mathbf{Y}')] \\ & \times [3(4\pi)^{-2} d\Omega_\pi d\Omega_n d\cos\theta]. \end{aligned}$$

Each F_i is an unknown function of E and $\cos\theta$, and depends on the dynamics of the process.

It is convenient to introduce another parametrization of the cross-section formula:

$$\begin{aligned} d^5\sigma = & C(E, \cos\theta) [f_1(\mathbf{n} \cdot \mathbf{N})^2 + f_2(\mathbf{n} \cdot \mathbf{X})^2 + f_3(\mathbf{n} \cdot \mathbf{Y})^2 \\ & + f_4(\mathbf{n} \cdot \mathbf{X})(\mathbf{n} \cdot \mathbf{Y}) + f_5(\mathbf{n} \cdot \mathbf{N})^2(\boldsymbol{\pi} \cdot \mathbf{N}) + \dots] \\ & \times [3(4\pi)^{-2} d\Omega_\pi d\Omega_n d\cos\theta], \end{aligned}$$

with the subsidiary condition $f_1 + f_2 + f_3 = 1$, which is the normalization condition after integration over the two solid angles involved. By this parametrization we have provided a convenient normalization for the dependence of the cross section on the decay angles of the Λ and ω . That is, the dependence of the cross section on the decay angles (which means the dependence on the spin alignments of the Λ and ω) is contained in the $\{f_i\}$ in the form of a probability density whose integral is 1. Thus we have

$$\begin{aligned} d\sigma = & \int_{\Omega_\pi} \int_{\Omega_n} d^5\sigma \\ = & C(E, \cos\theta) d\cos\theta \iint [f_1(\mathbf{n} \cdot \mathbf{N})^2 + \dots] \frac{3}{(4\pi)^2} d\Omega_\pi d\Omega_n \\ = & C(E, \cos\theta) d\cos\theta. \end{aligned}$$

Thus $C(E, \cos\theta)$ is the differential cross section, inte-

¹³ N. Byers and C. N. Yang, Phys. Rev. **135**, B796 (1964).

¹⁴ S. M. Berman and R. J. Oakes, Phys. Rev. **135**, B1034 (1964).

¹⁵ R. W. Huff, Phys. Rev. **133**, B1078 (1964).

¹⁶ M. Ademollo and R. Gatto, Phys. Rev. **133**, B531 (1964).

grated over all decay angles, of the reaction taking place at a given E and $\cos\theta$.

The total cross section is given by

$$\sigma_T = \int C(E, \cos\theta) d\cos\theta.$$

D. General Model

At this point we might tabulate $d\sigma/d\cos\theta$ and the set of f_i as a function of E and $\cos\theta$. However, we still face the problem of choosing the vectors \mathbf{X}' , \mathbf{Y}' , and \mathbf{X} , \mathbf{Y} in the Λ and the ω rest frames, respectively. If we could do our experiment at a unique E and a unique θ , then, in each frame, any choice would be related to any other by a simple rotation around the normal. However, since we must average over regions of E and $\cos\theta$, it behooves us to choose our axes carefully. The choice is determined by the characteristics of the model being tested.

Most current theories have as a basis the idea of exchanged particles, as expressed, for example, in Feynman diagrams or unitarity graphs. Figures 7(a), 7(b), and 7(c) represent exchanges of the least-massive particles allowed in the three possible channels in $Kp \rightarrow \Lambda\omega$ —the s , t , and u channels. With this model the correct choice of axes is apparent. In the u channel the appropriate axes in the ω rest frame are \mathbf{p} , $\mathbf{N} \times \mathbf{p}$, and \mathbf{N} , and in the Λ rest frame they are \mathbf{K} , $\mathbf{N} \times \mathbf{K}$, and \mathbf{N} . In the t channel, the two sets are \mathbf{K} , $\mathbf{N} \times \mathbf{K}$, and \mathbf{N} , and \mathbf{p} , $\mathbf{N} \times \mathbf{p}$, and \mathbf{N} . In the s channel we have $\mathbf{\Lambda}$, $\mathbf{N} \times \mathbf{\Lambda}$, and \mathbf{N} , and $\mathbf{\omega}$, $\mathbf{N} \times \mathbf{\omega}$, and \mathbf{N} . In this article we concern ourselves, in the section on the absorption model, with t -channel exchanges of pseudoscalar and vector mesons. We therefore tabulate our data with the $\{f_i\}$ determined with axes appropriate to the t channel. We iterate that the $\{f_i\}$, if they were obtained at a unique E and θ , would be related to the u and s channel $\{f_i\}$ by a simple rotation.

E. Experimental Calculations

The quantities $d\sigma/d\cos\theta$ and σ_T were obtained by a simple counting of events in a given region of E and $\cos\theta$. The only problem here is background subtraction, which is discussed in the next section.

The maximum-likelihood technique was used to determine $\{f_i\}$. For each event we have a probability density that is a function of the twelve f_i ,

$$P_k = f_1(\mathbf{n} \cdot \mathbf{N})_k^2 + f_2(\mathbf{n} \cdot \mathbf{X})_k^2 + f_3(\mathbf{n} \cdot \mathbf{Y})_k^2 + \dots,$$

where the vectors have been evaluated for the particular event, as the subscript k indicates.

For a sample of N events, the likelihood is,

$$\mathcal{L} = \prod_{k=1}^N P_k.$$

We maximize \mathcal{L} by maximizing

$$\ln \mathcal{L} = \sum_{k=1}^N \ln P_k.$$

We vary only 11 of the parameters $\{f_i\}$, since there is one constraint. Only one extremum can exist for our likelihood, and it is a maximum. Both of these facts are a consequence of the linearity of P_k as a function of the parameters $\{f_i\}$.

F. Background

If we look at the three-pion mass spectra in the reaction $Kp \rightarrow \Lambda\pi^+\pi^-\pi^0$, we see a prominent ω peak (see Figs. 14 through 17). Under this peak we also see a significant background, which we judged from the regions adjacent to the peak. By sketching a curve through the regions next to the ω peak, we estimate the number of non- ω events in the region of the three-pion mass between 750 and 810 MeV. We assume that the

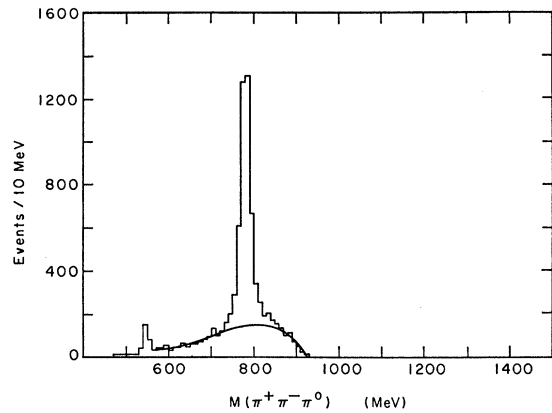


FIG. 14. Three-pion mass distributions for 7720 $Kp \rightarrow \Lambda\pi^+\pi^-\pi^0$ events at 1.5 BeV/c. The curves in this and the next three plots are hand-drawn estimates of background under the ω peak.

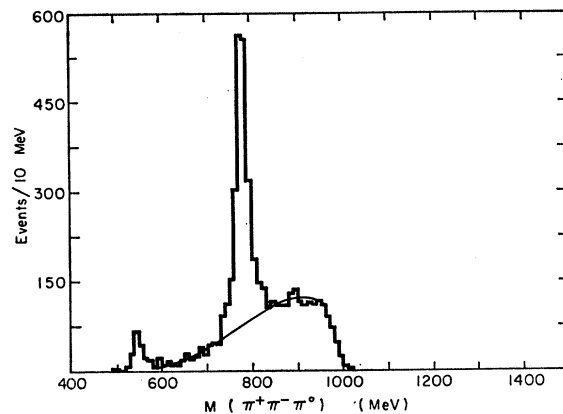


FIG. 15. Three-pion mass distributions for 4900 $Kp \rightarrow \Lambda\pi^+\pi^-\pi^0$ events at 1.7 BeV/c.

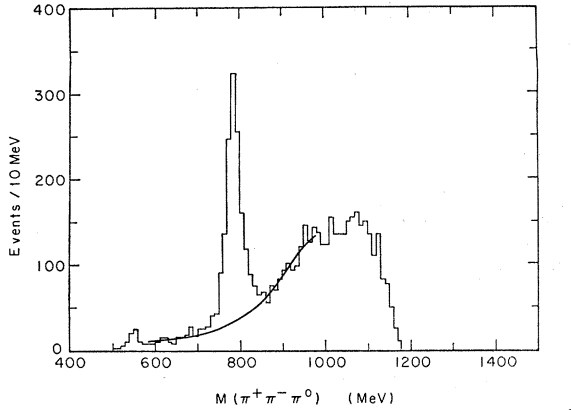


FIG. 16. Three-pion mass distributions for 5560 $K^-p \rightarrow \Lambda\pi^+\pi^-\pi^0$ events at 2.1 BeV/c.

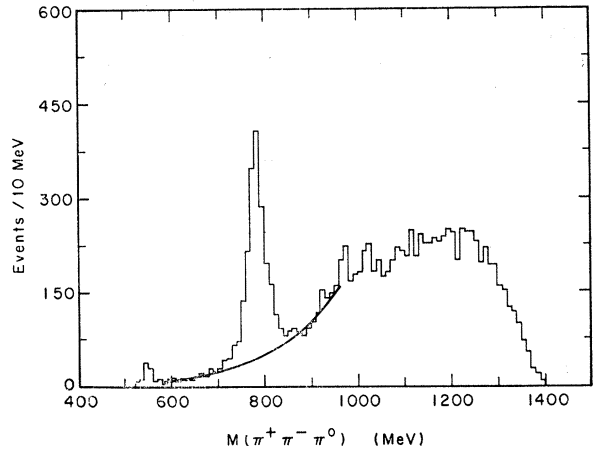


FIG. 17. Three-pion mass distributions for 11 830 $K^-p \rightarrow \Lambda\pi^+\pi^-\pi^0$ events at 2.6 BeV/c. The statistically significant peaks at 960 and 1020 MeV are the $\pi^+\pi^-\gamma$ decays of the $\eta(959)$ and the 3π decay of the ϕ , respectively.

remainder in this region represent events of the reaction $Kp \rightarrow \Lambda\omega$.

Let us call the 750- to 810-MeV region the ω region, and the two regions 690 to 750 MeV and 810 to 870 MeV, combined, the control region. Let N_B be the

number of background events in the ω region, and N_C the number of events in the control region. We are dealing with a spectrum at a given E . To find the number of ω events N_ω in a certain region of $\cos\theta$, we use $N_\omega = N - (N_B/N_C)(M)$, where N is the number of events in the ω region and in the region of $\cos\theta$ under discussion, and M is the number of events in the control region and in the region of $\cos\theta$ under discussion.

Treating background in determinations of $\{f_i\}$ is only slightly more complicated. The $\{f_i\}_\omega$ for events in the ω region is determined with the technique described in Sec. E and another set $\{f_i\}_c$ is determined for the events in the control region. Both sets are normalized to a total integral of one, so that the expression for the $\{f_i\}$ for the ω events is

$$f_i = (1/N_\omega)\{Nf_{i\omega} - (N_B/N_C)(M)f_{ic}\}.$$

G. Errors

The errors on cross sections are treated in the usual manner for counting experiments. The errors on the f_i are more complex. The maximum-likelihood routine we used yields an error matrix (obtained from inverting the second-derivative matrix) for the 11 f_i that were varied in the search. Thus we have all the correlated errors, and since the 12th parameter is a function of the other 11 ($f_{12} = 1 - f_2 - f_3$), we may find its error correlations also. When we list the error, σ_{f_i} , for an f_i , we are listing the square root of the diagonal element of the error matrix corresponding to that f_i . Thus the error matrix is

$$\langle \delta f_i \delta f_j \rangle = \frac{1}{(N_\omega)^2} \left[N^2 \langle \delta f_{i\omega} \delta f_{j\omega} \rangle - \left(\frac{N_B M}{N_C} \right)^2 \langle \delta f_{ic} \delta f_{jc} \rangle \right]$$

and

$$\sigma_{f_i} = \langle (\delta f_i)^2 \rangle^{1/2}.$$

Because of space limitations we have provided only the error matrices for the forward direction at 2.6 BeV/c.

H. Presentation of Data

Figure 8 shows that our data lie in four distinct regions of c.m. energy. The exposures at 1.95 and

TABLE III. Correlation parameters for incident K^- laboratory momentum ≈ 1.5 BeV/c. The c.m. energy is ≈ 2.02 BeV. The total cross section for $K^-p \rightarrow \Lambda\omega \rightarrow \Lambda\pi^+\pi^-\pi^0$ near 1.5 BeV/c is 0.96 ± 0.05 mb. The total number of ω events at all $\cos\theta$ is 3568.

	1.00	0.75	0.50	0.25	0.00	-0.25	-0.50	-0.75	-1.00
$\cos\theta_{\max}$	1.00	0.75	0.50	0.25	0.00	-0.25	-0.50	-0.75	-1.00
$\cos\theta_{\min}$	0.75	0.50	0.25	0.00	-0.25	-0.50	-0.75	-1.00	-1.00
$N(E, \cos\theta)^a$	704	770	818	694	550	414	310	237	237
$C(E, \cos\theta)^b$	262	244	253	245	207	261	252	248	248
f_1	0.279 ± 0.034	0.260 ± 0.031	0.222 ± 0.029	0.188 ± 0.031	0.302 ± 0.039	0.426 ± 0.053	0.359 ± 0.070	0.489 ± 0.100	0.489 ± 0.100
f_2	0.392 ± 0.034	0.500 ± 0.033	0.599 ± 0.032	0.571 ± 0.035	0.551 ± 0.039	0.420 ± 0.054	0.479 ± 0.072	0.336 ± 0.091	0.336 ± 0.091
f_3	0.329 ± 0.033	0.240 ± 0.031	0.179 ± 0.028	0.241 ± 0.032	0.147 ± 0.034	0.154 ± 0.048	0.162 ± 0.066	0.175 ± 0.092	0.175 ± 0.092
f_4	0.288 ± 0.059	0.313 ± 0.053	0.369 ± 0.048	0.385 ± 0.057	0.350 ± 0.064	0.376 ± 0.087	0.148 ± 0.116	-0.162 ± 0.179	-0.162 ± 0.179
f_5	-0.053 ± 0.064	-0.099 ± 0.053	-0.101 ± 0.050	-0.007 ± 0.055	0.059 ± 0.077	0.011 ± 0.106	0.118 ± 0.133	0.414 ± 0.174	0.414 ± 0.174
f_6	-0.299 ± 0.062	-0.066 ± 0.065	-0.137 ± 0.066	-0.240 ± 0.070	-0.250 ± 0.079	-0.032 ± 0.107	0.138 ± 0.136	-0.219 ± 0.166	-0.219 ± 0.166
f_7	0.027 ± 0.059	0.021 ± 0.057	0.084 ± 0.052	0.101 ± 0.055	-0.013 ± 0.062	0.051 ± 0.082	0.106 ± 0.133	-0.249 ± 0.163	-0.249 ± 0.163
f_8	-0.540 ± 0.101	-0.118 ± 0.091	-0.259 ± 0.085	-0.130 ± 0.098	-0.192 ± 0.110	-0.322 ± 0.154	-0.405 ± 0.189	-0.147 ± 0.294	-0.147 ± 0.294
f_9	0.204 ± 0.101	0.244 ± 0.102	0.318 ± 0.091	0.005 ± 0.104	-0.267 ± 0.120	0.139 ± 0.161	-0.143 ± 0.228	-0.743 ± 0.307	-0.743 ± 0.307
f_{10}	-0.077 ± 0.110	-0.091 ± 0.092	-0.087 ± 0.080	-0.074 ± 0.090	-0.244 ± 0.105	0.160 ± 0.156	0.471 ± 0.208	0.118 ± 0.284	0.118 ± 0.284
f_{11}	-0.197 ± 0.091	-0.179 ± 0.094	-0.014 ± 0.093	0.016 ± 0.105	0.289 ± 0.119	0.072 ± 0.164	0.439 ± 0.225	0.298 ± 0.288	0.298 ± 0.288
f_{12}	0.191 ± 0.096	0.139 ± 0.083	0.210 ± 0.083	0.333 ± 0.088	0.127 ± 0.103	0.407 ± 0.148	0.396 ± 0.186	0.178 ± 0.300	0.178 ± 0.300

^a N is the number of events in the ω region.

^b C is the number of events in the control region.

TABLE IV. Correlation parameters for incident K^- laboratory momentum ≈ 1.7 BeV/c. The c.m. energy is ≈ 2.10 BeV. The total cross section for $K^-p \rightarrow \Lambda\omega \rightarrow \Lambda\pi^+\pi^-\pi^0$ near 1.7 BeV/c is 0.80 ± 0.15 mb. The total number of ω events at all $\cos\theta$ is 1566.

$\cos\theta_{\max}$	1.00	0.75	0.50	0.25	0.00	-0.25	-0.50	-0.75	-0.75
$\cos\theta_{\min}$	0.75	0.50	0.25	0.00	-0.25	-0.50	-0.75	-1.00	-1.00
$N(E, \cos\theta)^a$	389	425	394	366	330	335	306	266	266
$C(E, \cos\theta)^b$	218	174	163	194	161	163	238	232	232
f_1	0.350 \pm 0.053	0.178 \pm 0.041	0.280 \pm 0.045	0.206 \pm 0.047	0.142 \pm 0.048	0.333 \pm 0.051	0.256 \pm 0.065	0.245 \pm 0.070	0.245 \pm 0.070
f_2	0.418 \pm 0.050	0.664 \pm 0.046	0.587 \pm 0.048	0.539 \pm 0.053	0.477 \pm 0.052	0.411 \pm 0.051	0.589 \pm 0.067	0.411 \pm 0.073	0.411 \pm 0.073
f_3	0.232 \pm 0.049	0.158 \pm 0.039	0.133 \pm 0.042	0.255 \pm 0.050	0.380 \pm 0.054	0.255 \pm 0.050	0.154 \pm 0.060	0.304 \pm 0.074	0.304 \pm 0.074
f_4	0.253 \pm 0.086	0.227 \pm 0.076	0.312 \pm 0.076	-0.109 \pm 0.091	0.189 \pm 0.098	0.419 \pm 0.087	0.211 \pm 0.117	-0.211 \pm 0.121	-0.211 \pm 0.121
f_5	-0.092 \pm 0.100	0.100 \pm 0.076	-0.133 \pm 0.074	-0.124 \pm 0.081	-0.137 \pm 0.086	-0.006 \pm 0.098	0.068 \pm 0.107	0.370 \pm 0.137	0.370 \pm 0.137
f_6	-0.042 \pm 0.097	0.002 \pm 0.099	0.087 \pm 0.103	0.095 \pm 0.115	-0.190 \pm 0.113	0.136 \pm 0.103	0.070 \pm 0.146	-0.040 \pm 0.155	-0.040 \pm 0.155
f_7	-0.048 \pm 0.086	-0.162 \pm 0.074	0.057 \pm 0.070	-0.008 \pm 0.090	0.149 \pm 0.106	0.058 \pm 0.082	0.087 \pm 0.117	0.124 \pm 0.139	0.124 \pm 0.139
f_8	-0.603 \pm 0.133	-0.009 \pm 0.128	-0.089 \pm 0.132	-0.002 \pm 0.151	-0.040 \pm 0.181	0.120 \pm 0.155	-0.259 \pm 0.195	-0.374 \pm 0.198	-0.374 \pm 0.198
f_9	0.307 \pm 0.165	0.261 \pm 0.139	0.094 \pm 0.155	0.269 \pm 0.161	-0.081 \pm 0.173	0.033 \pm 0.165	-0.281 \pm 0.201	-0.040 \pm 0.251	-0.040 \pm 0.251
f_{10}	-0.205 \pm 0.139	-0.199 \pm 0.131	-0.056 \pm 0.130	-0.205 \pm 0.141	-0.277 \pm 0.132	-0.276 \pm 0.153	-0.274 \pm 0.188	0.351 \pm 0.211	0.351 \pm 0.211
f_{11}	-0.033 \pm 0.148	0.179 \pm 0.131	0.189 \pm 0.147	-0.156 \pm 0.146	0.014 \pm 0.156	0.175 \pm 0.162	0.676 \pm 0.183	0.762 \pm 0.243	0.762 \pm 0.243
f_{12}	-0.069 \pm 0.153	0.145 \pm 0.121	0.041 \pm 0.113	0.091 \pm 0.144	0.190 \pm 0.133	0.351 \pm 0.141	0.370 \pm 0.174	0.462 \pm 0.194	0.462 \pm 0.194

^a N is the number of events in the ω region.^b C is the number of events in the control region.TABLE V. Correlation parameters for incident K^- laboratory momentum ≈ 2.1 BeV/c. The c.m. energy is ≈ 2.27 BeV. The total cross section for $K^-p \rightarrow \Lambda\omega \rightarrow \Lambda\pi^+\pi^-\pi^0$ near 2.1 BeV/c is 0.48 ± 0.05 mb. The total number of ω events at all $\cos\theta$ is 1021.

$\cos\theta_{\max}$	1.00	0.75	0.50	0.25	0.00	-0.25	-0.50	-0.75	-0.75
$\cos\theta_{\min}$	0.75	0.50	0.25	0.00	-0.25	-0.50	-0.75	-1.00	-1.00
$N(E, \cos\theta)^a$	122	123	156	143	165	188	161	152	152
$C(E, \cos\theta)^b$	84	87	73	60	75	94	99	101	101
f_1	0.572 \pm 0.090	0.433 \pm 0.097	0.370 \pm 0.072	0.331 \pm 0.070	0.181 \pm 0.059	0.190 \pm 0.056	0.263 \pm 0.073	0.261 \pm 0.072	0.261 \pm 0.072
f_2	0.105 \pm 0.071	0.237 \pm 0.090	0.249 \pm 0.069	0.299 \pm 0.066	0.521 \pm 0.066	0.624 \pm 0.061	0.366 \pm 0.075	0.302 \pm 0.075	0.302 \pm 0.075
f_3	0.323 \pm 0.085	0.330 \pm 0.089	0.381 \pm 0.071	0.370 \pm 0.073	0.298 \pm 0.059	0.186 \pm 0.055	0.371 \pm 0.071	0.437 \pm 0.079	0.437 \pm 0.079
f_4	0.013 \pm 0.145	0.334 \pm 0.135	0.271 \pm 0.119	0.547 \pm 0.113	0.514 \pm 0.127	0.169 \pm 0.118	0.088 \pm 0.141	-0.092 \pm 0.136	-0.092 \pm 0.136
f_5	-0.039 \pm 0.186	-0.002 \pm 0.195	-0.245 \pm 0.126	0.033 \pm 0.128	-0.009 \pm 0.123	-0.124 \pm 0.120	-0.143 \pm 0.136	0.193 \pm 0.150	0.193 \pm 0.150
f_6	-0.031 \pm 0.125	0.313 \pm 0.172	-0.000 \pm 0.122	0.253 \pm 0.111	0.146 \pm 0.138	0.209 \pm 0.128	0.003 \pm 0.148	-0.080 \pm 0.138	-0.080 \pm 0.138
f_7	0.005 \pm 0.147	-0.222 \pm 0.152	0.022 \pm 0.147	-0.006 \pm 0.145	-0.062 \pm 0.125	0.173 \pm 0.093	-0.129 \pm 0.136	0.248 \pm 0.152	0.248 \pm 0.152
f_8	-0.313 \pm 0.235	-0.252 \pm 0.262	0.153 \pm 0.213	0.512 \pm 0.224	0.507 \pm 0.237	-0.039 \pm 0.186	-0.076 \pm 0.240	-0.144 \pm 0.228	-0.144 \pm 0.228
f_9	0.257 \pm 0.255	0.114 \pm 0.245	0.083 \pm 0.207	0.472 \pm 0.205	0.021 \pm 0.194	0.265 \pm 0.182	-0.356 \pm 0.201	-0.158 \pm 0.235	-0.158 \pm 0.235
f_{10}	-0.455 \pm 0.280	-0.123 \pm 0.272	0.292 \pm 0.231	-0.021 \pm 0.216	-0.281 \pm 0.212	-0.210 \pm 0.141	0.062 \pm 0.229	-0.019 \pm 0.262	-0.019 \pm 0.262
f_{11}	0.515 \pm 0.245	0.263 \pm 0.229	0.187 \pm 0.199	0.371 \pm 0.214	-0.308 \pm 0.194	-0.760 \pm 0.205	-0.300 \pm 0.185	-0.095 \pm 0.224	-0.095 \pm 0.224
f_{12}	-0.181 \pm 0.284	0.365 \pm 0.287	-0.173 \pm 0.202	-0.017 \pm 0.210	-0.082 \pm 0.208	-0.119 \pm 0.191	0.107 \pm 0.244	0.241 \pm 0.207	0.241 \pm 0.207

^a N is the number of events in the ω region.^b C is the number of events in the control region.TABLE VI. Correlation parameters for incident K^- laboratory momentum ≈ 2.6 BeV/c. The c.m. energy is ≈ 2.49 BeV. The total cross section for $K^-p \rightarrow \Lambda\omega \rightarrow \Lambda\pi^+\pi^-\pi^0$ near 2.6 BeV/c is 0.22 ± 0.03 mb. The total number of ω events at all $\cos\theta$ is 1300.

$\cos\theta_{\max}$	1.00	0.75	0.50	0.25	0.00	-0.25	-0.50	-0.75	-0.75
$\cos\theta_{\min}$	0.75	0.50	0.25	0.00	-0.25	-0.50	-0.75	-1.00	-1.00
$N(E, \cos\theta)^a$	435	180	132	123	118	180	210	201	201
$C(E, \cos\theta)^b$	145	115	74	79	84	111	122	168	168
f_1	0.504 \pm 0.041	0.586 \pm 0.069	0.517 \pm 0.082	0.271 \pm 0.092	0.317 \pm 0.094	0.125 \pm 0.058	0.112 \pm 0.057	0.374 \pm 0.075	0.374 \pm 0.075
f_2	0.397 \pm 0.041	0.349 \pm 0.072	0.348 \pm 0.083	0.149 \pm 0.072	0.465 \pm 0.101	0.359 \pm 0.071	0.320 \pm 0.067	0.251 \pm 0.074	0.251 \pm 0.074
f_3	0.099 \pm 0.030	0.065 \pm 0.062	0.134 \pm 0.070	0.580 \pm 0.090	0.218 \pm 0.089	0.516 \pm 0.069	0.368 \pm 0.070	0.375 \pm 0.078	0.375 \pm 0.078
f_4	0.132 \pm 0.062	0.226 \pm 0.098	0.200 \pm 0.133	0.242 \pm 0.167	0.317 \pm 0.150	0.376 \pm 0.128	0.361 \pm 0.109	0.032 \pm 0.132	0.032 \pm 0.132
f_5	-0.185 \pm 0.085	-0.474 \pm 0.143	-0.436 \pm 0.178	0.210 \pm 0.163	0.150 \pm 0.202	-0.006 \pm 0.104	0.014 \pm 0.098	0.384 \pm 0.111	0.384 \pm 0.111
f_6	0.059 \pm 0.079	0.293 \pm 0.152	0.032 \pm 0.176	0.231 \pm 0.113	0.490 \pm 0.204	0.028 \pm 0.142	0.188 \pm 0.142	-0.039 \pm 0.134	-0.039 \pm 0.134
f_7	-0.045 \pm 0.062	-0.140 \pm 0.102	0.300 \pm 0.170	0.379 \pm 0.187	0.076 \pm 0.148	-0.003 \pm 0.141	0.039 \pm 0.143	0.077 \pm 0.142	0.077 \pm 0.142
f_8	-0.248 \pm 0.103	-0.094 \pm 0.173	0.067 \pm 0.246	0.354 \pm 0.284	0.404 \pm 0.239	-0.089 \pm 0.224	-0.085 \pm 0.187	-0.025 \pm 0.231	-0.025 \pm 0.231
f_9	-0.001 \pm 0.138	-0.509 \pm 0.235	-0.526 \pm 0.267	0.321 \pm 0.241	0.278 \pm 0.245	0.031 \pm 0.183	0.029 \pm 0.176	-0.211 \pm 0.231	-0.211 \pm 0.231
f_{10}	-0.043 \pm 0.119	-0.265 \pm 0.212	0.213 \pm 0.289	-0.052 \pm 0.258	0.092 \pm 0.293	-0.351 \pm 0.218	-0.273 \pm 0.191	-0.086 \pm 0.221	-0.086 \pm 0.221
f_{11}	-0.033 \pm 0.126	0.224 \pm 0.246	-0.226 \pm 0.222	0.436 \pm 0.252	-0.171 \pm 0.281	-0.286 \pm 0.185	-0.234 \pm 0.148	0.262 \pm 0.209	0.262 \pm 0.209
f_{12}	0.218 \pm 0.110	0.405 \pm 0.184	0.311 \pm 0.206	0.201 \pm 0.259	0.342 \pm 0.312	-0.189 \pm 0.229	0.370 \pm 0.143	0.523 \pm 0.223	0.523 \pm 0.223

^a N is the number of events in the ω region.^b C is the number of events in the control region.

2.41 BeV do not comprise enough data to meaningfully determine the many parameters of the angular distributions. Therefore we have separated the data into four sections corresponding to the beam momentum settings 1.2 to 1.5 BeV/c, 1.6 to 1.7 BeV/c, 2.1 BeV/c, and 2.4 to 2.7 BeV/c. Figures 3 through 6 show the distributions in production angle for each of the four regions. Figures 18 through 21 as well as Tables III through VIII give the decay correlations $\{f_i\}$ determined in many intervals of production angle for each of the four regions. Thus Figs. 3 through 6 and 18

through 21, along with the total cross sections shown in Fig. 2, present the entire range of knowledge available about this reaction in our experiment, and in fact represent the entire extent of the information obtainable about the production mechanisms in this reaction from film of a bubble chamber with unpolarized protons.

IV. THEORY OF THE ABSORPTION MODEL

A. Introduction

Reactions involving two particles in the initial state and two particles in the final state generally show a

TABLE VII. 2.6-BeV/c correlation parameters for forward production angles.

$\cos\theta_{\max}$	1.00	0.875	0.75
$\cos\theta_{\min}$	0.875	0.75	0.625
$N(E, \cos\theta)^a$	252	183	118
$C(E, \cos\theta)^b$	83	62	66
f_1	0.464 ± 0.054	0.546 ± 0.060	0.667 ± 0.080
f_2	0.414 ± 0.053	0.378 ± 0.062	0.325 ± 0.090
f_3	0.121 ± 0.041	0.076 ± 0.039	0.008 ± 0.067
f_4	0.197 ± 0.086	0.077 ± 0.090	0.098 ± 0.119
f_5	-0.166 ± 0.107	-0.297 ± 0.137	-0.418 ± 0.177
f_6	0.091 ± 0.096	-0.022 ± 0.127	0.148 ± 0.181
f_7	0.085 ± 0.099	-0.085 ± 0.086	-0.029 ± 0.119
f_8	-0.387 ± 0.156	-0.186 ± 0.166	0.014 ± 0.218
f_9	0.133 ± 0.180	-0.174 ± 0.212	-0.163 ± 0.298
f_{10}	-0.032 ± 0.153	0.101 ± 0.190	-0.508 ± 0.306
f_{11}	0.068 ± 0.166	-0.215 ± 0.192	0.332 ± 0.312
f_{12}	0.065 ± 0.138	0.588 ± 0.200	0.486 ± 0.246

^a N is the number of events in the ω region.

^b C is the number of events in the control region.

peaking at small momentum transfers, or equivalently, at forward production angles, at least at energies large enough to avoid threshold effects. The characteristic dominance of small production angles has been explained on the basis of long-range forces—the one-particle-exchange model.¹⁷ [See Fig. 1(a)]. However, the quantitative calculation of the appropriate Feynman diagrams generally results in a production-angle distribution that is not as forward peaked as the data and in a cross section that is larger by an order of magnitude than the data. One can say equivalently that the theoretical predictions with low partial waves removed would fit the data.

TABLE VIII. Error matrices for 2.6 BeV/c data in the forward direction; $10^6 \langle \delta f_i \delta f_j \rangle$.

0.875 < $\cos\theta$ < 1.00												
	f_1	f_2	f_3	f_4	f_5	f_6	f_7	f_8	f_9	f_{10}	f_{11}	f_{12}
f_1	2956	-2031	-925	-601	-572	1	-37	857	227	-466	597	254
f_2		2777	-745	171	442	234	-199	-973	-243	170	-650	-386
f_3			1671	430	130	-235	236	116	17	296	53	132
f_4				7380	82	-1271	-65	428	418	178	379	111
f_5					11 435	-2221	-2923	-567	108	-737	-448	-504
f_6						9305	-2478	2342	320	-1008	1302	787
f_7							9817	-926	1106	3108	679	-647
f_8								24 396	-796	1432	945	2712
f_9									32 538	2368	-223	-501
f_{10}										23 460	-210	-981
f_{11}											27 419	4294
f_{12}												19 155
0.75 < $\cos\theta$ < 0.875												
	f_1	f_2	f_3	f_4	f_5	f_6	f_7	f_8	f_9	f_{10}	f_{11}	f_{12}
f_1	3607	-2998	-609	-982	-1500	353	645	934	1824	380	70	668
f_2		3877	879	84	1072	-429	23	-1025	-1888	-199	-62	-2368
f_3			1488	898	428	77	-671	91	64	-181	-7	1700
f_4				8021	354	-1496	166	-1234	-378	-2319	2154	-1203
f_5					18 774	-4705	-2270	-3509	2390	-2654	-537	-1034
f_6						16 069	-3106	-80	1668	1054	-297	-386
f_7							7460	5651	-11	148	-12	2360
f_8								27 665	305	1964	-249	3794
f_9									45 092	-2460	3443	3848
f_{10}										36 189	1898	9895
f_{11}											36 992	-2490
f_{12}												40 038

¹⁷ For references to the one-particle-exchange model and its modifications, such as form factors, absorption, and Regge poles, see Ref. 3.

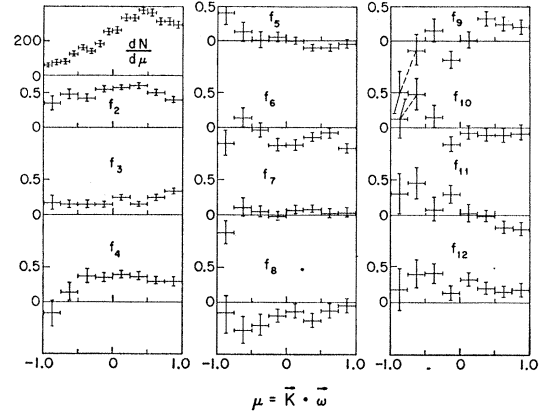


FIG. 18. Distributions of the number of events and the decay correlations $\{f_i\}$ as a function of production-angle cosine for $K^-p \rightarrow \Lambda\omega$ events at 1.5 BeV/c. Dashed lines are used to eliminate possible confusion.

A natural explanation for a dearth of low partial waves is absorption. That is, more complicated reactions go through small impact parameters and thus compete with the two-body final state in low partial waves. This competition effectively reduces the low partial-wave components of the two-body final state. The absorption model is a quantitative treatment of the foregoing idea.³

B. Formalism

We use a formalism developed by Huff,⁷ which uses a linear-momentum representation rather than the more usual angular-momentum representation. Since Huff's

results have not been published, we briefly outline his methods and equations.

First we must find the amplitudes for the Feynman diagrams corresponding to Fig. 1(a) with particle e being either a K or a K^* meson. These amplitudes are called the Born amplitudes. Let B_{ij} be the Born amplitude taking into account both K and K^* exchange where the initial proton has helicity plus, the final ω has helicity i , and the final Λ has helicity j . The amplitudes for an initial proton with helicity minus are related to the B_{ij} by parity conservation. Then the six independent Born amplitudes are given by:

$$B_{++} = G_1\{(C_-/\sqrt{2})p_2m_3\sin\theta\} + G_2\{- (C_+/\sqrt{2})Q_2 \\ -\sqrt{2}D_+Q_1 - \sqrt{2}D_-E_{e.m.}(p_2p_4\sin\theta)[(m_2+m_4)/\alpha]\} \\ + G_3\{\sqrt{2}D_-E_{e.m.}(p_2p_4\sin\theta)(m_2+m_4)^{-1}\},$$

$$B_{0+} = G_1\{-C_-Q_2\} + G_2\{-C_+p_2m_3\sin\theta\},$$

$$B_{-+} = G_1\{- (C_-/\sqrt{2})p_2m_3\sin\theta\} + G_2\{(C_+/\sqrt{2})Q_2 \\ -\sqrt{2}D_+Q_1 - \sqrt{2}D_-E_{e.m.}(p_2p_4\sin\theta)[(m_2+m_4)/\alpha]\} \\ + G_3\{\sqrt{2}D_-E_{e.m.}(p_2p_4\sin\theta)(m_2+m_4)^{-1}\},$$

$$B_{+-} = G_1\{(C_+/\sqrt{2})p_2m_3\sin\theta\} + G_2\{(C_-/\sqrt{2})Q_2 - \sqrt{2}D_-Q_1 \\ + \sqrt{2}D_+E_{e.m.}(p_2p_4\sin\theta)[(m_2+m_4)/\alpha]\} \\ + G_3\{-\sqrt{2}D_+E_{e.m.}(p_2p_4\sin\theta)(m_2+m_4)^{-1}\},$$

$$B_{0-} = G_1\{-C_+Q_2\} + G_2\{C_-p_2m_3\sin\theta\},$$

$$B_{--} = G_1\{- (C_+/\sqrt{2})p_2m_3\sin\theta\} + G_2\{- (C_-/\sqrt{2})Q_2 \\ -\sqrt{2}D_-Q_1 + \sqrt{2}D_+E_{e.m.}(p_2p_4\sin\theta)[(m_2+m_4)/\alpha]\} \\ + G_3\{-\sqrt{2}D_+E_{e.m.}(p_2p_4\sin\theta)(m_2+m_4)^{-1}\},$$

where

$$G_1 = \frac{G(\omega K^+ K^-)G(\bar{p} K^+ \Lambda)}{4\pi(m_{K^*}^2 - t)}(2\beta),$$

$$G_2 = \frac{G(\omega K^+ K^*)[G_V(\bar{p} K^* + \Lambda) + G_T(\bar{p} K^* + \Lambda)]}{4\pi(m_{K^*}^2 - t)}\beta,$$

$$G_3 = \frac{G(\omega K^+ K^*)G_T(\bar{p} K^* + \Lambda)}{4\pi(m_{K^*}^2 - t)}\beta,$$

$$Q_1 = \frac{1}{2}[E_{e.m.}(E_2 + E_4) - \frac{1}{2}\alpha + 2m_2m_4] \\ - [(m_1 + m_3)/\alpha]E_{e.m.}(m_2E_4 + m_4E_2),$$

$$Q_2 = E_1p_4 - E_3p_2\cos\theta,$$

$$\alpha = 2E_2E_4 + 2m_2m_4 - 2p_2p_4\cos\theta,$$

$$C_{\pm} = (1 \mp \cos\theta)^{1/2}\{[p_4/(m_4 + E_4)] \pm [p_2/(m_2 + E_2)]\},$$

$$D_{\pm} = (1 \mp \cos\theta)^{1/2}\{1 \pm [p_2p_4/(m_4 + E_4)(m_2 + E_2)]\},$$

$$\beta = \left[\frac{(E_4 + m_4)(E_2 + m_2)}{2m_3^2} \right]^{1/2},$$

$$t = m_1^2 + m_3^2 - 2E_1E_3 + 2p_1p_3\cos\theta,$$

$$\cos\theta = \mathbf{p}_1 \cdot \mathbf{p}_2,$$

$$p_i = |\mathbf{p}_i|,$$

$$E_i = (p_i^2 + m_i^2)^{1/2}.$$

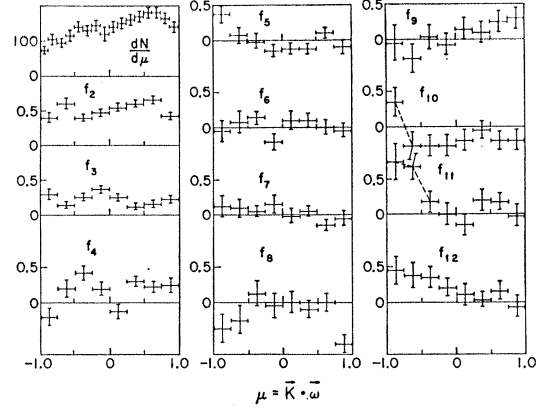


FIG. 19. Distributions of the number of events and the decay correlations $\{f_i\}$ as a function of production-angle cosine for $K^-p \rightarrow \Lambda\omega$ events at 1.7 BeV/c. Dashed lines are used to eliminate possible confusion.

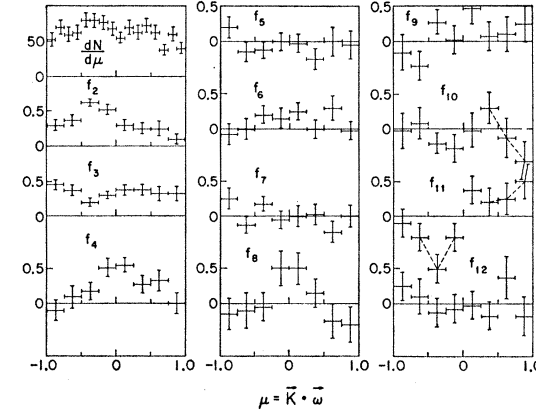


FIG. 20. Distributions of the number of events and the decay correlations $\{f_i\}$ as a function of production-angle cosine for $K^-p \rightarrow \Lambda\omega$ events at 2.1 BeV/c. Dashed lines are used to eliminate possible confusion.

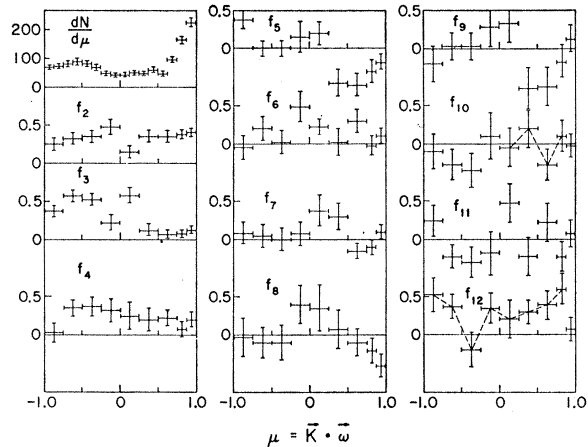


FIG. 21. Distributions of the number of events and the decay correlations $\{f_i\}$ as a function of production-angle cosine for $K^-p \rightarrow \Lambda\omega$ events at 2.6 BeV/c. Dashed lines are used to eliminate possible confusion.

Here the \mathbf{p}_i with $i=1, 2, 3$, or 4 correspond to the c.m. momenta for the K^- , p , ω , and Λ , respectively; $E_{\text{c.m.}}$ is the total energy in the c.m. system, and the coupling constants $G(abc)$ are as defined by Jackson and Pilkuhn.¹⁸

The differential cross section in terms of these Born amplitudes is

$$\frac{d\sigma}{d\Omega} = \frac{1}{4(E_{\text{c.m.}})^2} \frac{q'}{q} \sum_{i,j} |B_{ij}|^2,$$

where q and q' are the c.m. momenta in the initial and final states, respectively.

We agree that the B_{ij} are not the correct amplitudes for the reaction $K^-p \rightarrow \Lambda\omega$ even if this reaction takes place only by K and K^* exchange. The Born amplitudes must be modified by absorption.

The basic formula relied upon to correctly give the amplitude A_{ij} is, in matrix form,

$$A = S_f^{1/2} B S_i^{1/2}, \quad (1)$$

which is the high-energy equivalent of the distorted-wave Born approximation.¹⁹ The $S_i(S_f)$ is the S -matrix element for the elastic scattering between the two particles in the initial (final) state. In other words, this extension of the distorted-wave Born approximation is equivalent to including in our calculations the Feynman diagrams represented in Fig. 1(b). Omnes²⁰ has asserted that this equation is not valid in high-energy peripheral collisions involving low partial waves. However, he admits that the general effect of the modification to the Born amplitude that this equation implies, namely depletion of low partial waves, should indeed actually appear because of absorption. In the opinion of Ball and Frazer, this equation is fairly plausible within the S -matrix theory when the exchanged meson has spin zero. They find it impossible to justify for vector-meson exchange. They also assert, along with Omnes, that the approximations are easier to justify for high than for low partial waves. The marked success of the equation is reason enough to try it here.

We may exhibit the matrix character of Eq. (1) by expanding the equation in either the angular- or linear-momentum representations.

(1) *Angular-momentum representation.* Let

$$|a\rangle \equiv |i, J, M, \lambda_1, \lambda_2\rangle \quad \text{and} \quad |b\rangle \equiv |f, J, M, \lambda_3, \lambda_4\rangle$$

be initial and final states, with angular momentum J , M , and let the helicity of particle i be λ_i . The remaining

quantum numbers are contained in i, f :

$$\begin{aligned} & \langle fJM\lambda_3\lambda_4 | A | iJM\lambda_1\lambda_2 \rangle \\ &= \sum_{\{\lambda_i'\}} \langle fJM\lambda_3\lambda_4 | S_f^{1/2} | fJM\lambda_3'\lambda_4' \rangle \\ & \quad \times \langle fJM\lambda_3'\lambda_4' | B | iJM\lambda_1'\lambda_2' \rangle \\ & \quad \times \langle iJM\lambda_1'\lambda_2' | S_i^{1/2} | iJM\lambda_1\lambda_2 \rangle. \end{aligned}$$

(2) *Linear-momentum representation.* Expanding in a linear-momentum representation, we have

$$\begin{aligned} & \langle f\Omega\lambda_3\lambda_4 | A | i0\lambda_1\lambda_2 \rangle \\ &= \int d\Omega_f d\Omega_i \sum_{\{\lambda_i'\}} \langle f\Omega\lambda_3\lambda_4 | S_f^{1/2} | f\Omega_f\lambda_3'\lambda_4' \rangle \\ & \quad \times \langle f\Omega_f\lambda_3'\lambda_4' | B | i\Omega_i\lambda_1'\lambda_2' \rangle \langle i\Omega_i\lambda_1'\lambda_2' | S_i^{1/2} | i0\lambda_1\lambda_2 \rangle, \end{aligned}$$

where $|i\Omega\lambda_i\rangle$ is the state vector with the c.m. momentum vector in direction Ω .

The two representations are, of course, equivalent. However, significant differences arise in their application because different approximations are made. In the treatment of the $S^{1/2}$ matrix elements, for the angular-momentum applications³ it is assumed that the absorptivity is a function of the total angular momentum, whereas the more relevant variable is probably the orbital angular momentum. We do not have this problem with the linear-momentum application, but we must approximate the $S^{1/2}$ matrix elements in another way (see below). Some of the calculations done previously have approximated the partial wave sums by integrals that are equivalent to an impact-parameter approximation.⁵ This is completely avoided in the linear-momentum representation. But a number of calculations using Eq. (1) with exact partial-wave sums have been performed,²¹ and compare reasonably closely with the impact parameter method, at least for the type of reactions considered here. The chief difference between the angular-momentum and the linear-momentum representations is in the method of including the absorption, as will be discussed below.

To continue with the linear-momentum representation, we make the usual simplifying assumption that $\lambda_i' = \lambda_i$; that is, the elastic scattering in the initial and final states is all nonhelicity flip. Since the helicity-flip amplitudes must vanish in the forward direction, and the elastic-scattering differential cross sections extrapolate smoothly to near the optical-theorem point, this appears to be a reasonable assumption for the forward directions.

We must evaluate the matrix elements of $S^{1/2}$. We know that $S=1-T$, where T is the transition matrix, and the partial differential elastic cross sections are

¹⁸ J. D. Jackson and H. Pilkuhn, *Nuovo Cimento* **33**, 906 (1964).

¹⁹ See, for example, Ref. 20.

²⁰ Roland Omnes, *Phys. Rev.* **137**, B649 (1965).

²¹ H. Høgaasen and J. Høgaasen, *Nuovo Cimento* **40A**, 560 (1965); H. Høgaasen, J. Høgaasen, R. Keyser, and B. E. Y. Svensson, *ibid.* **42A**, 323 (1966); J. T. Donohue, Ph.D. thesis, University of Illinois, 1966 (unpublished).

given by

$$d\sigma_{\lambda_1\lambda_2}/d\Omega = |(2\pi/q)\langle i0\lambda_1\lambda_2 | T | i0\lambda_1\lambda_2 \rangle|^2.$$

Hence we have

$$\langle i0\lambda_1\lambda_2 | T | i0\lambda_1\lambda_2 \rangle = e^{i\psi} (q/2\pi) (d\sigma_{\lambda_1\lambda_2}/d\Omega)^{1/2},$$

where ψ is an unknown phase that is a function of production angle. If the elastic scattering is due completely to the absorption of inelastic scattering (i.e., elastic scattering is "shadow" scattering), then ψ is 0. However, even if the elastic cross sections extrapolate exactly to the optical-theorem point, $\psi \neq 0$ is still possible at $\theta \neq 0$ deg. Calculations up until now have assumed $\psi = 0$; however, we shall see in Sec. V that a nonzero value of ψ plays a crucial role in applying the absorption model to our data.

Under our assumptions, the differential elastic-scattering cross sections may be expressed by

$$\left(\frac{d\sigma}{d\Omega}\right)^{1/2} = \frac{\sigma_T q}{4\pi} e^{-A/2},$$

where σ_T is the total cross section for interaction between the two particles in the initial state. An analogous formula holds for the final state.

We approximate $S^{1/2}$ by

$$S^{1/2} = 1 - \frac{1}{2}T.$$

This approximation is equivalent to considering at most one elastic scatter in each of the blobs in Fig. 1(b).

We have now given enough information to construct the absorbed amplitude A . After properly taking into account the necessary rotations from various helicity frames to other helicity frames, Huff's final result is

$$\begin{aligned} &\langle f\Omega\lambda_3\lambda_4 | A | i0\lambda_1\lambda_2 \rangle \\ &= \langle f\Omega\lambda_3\lambda_4 | B | i0\lambda_1\lambda_2 \rangle \\ &- \frac{1}{2} \int d\Omega' \eta [\langle f\Omega'\lambda_3\lambda_4 | B | i0\lambda_1\lambda_2 \rangle \langle i\Omega\lambda_1\lambda_2 | T | i0\lambda_1\lambda_2 \rangle \\ &+ \langle f\Omega'\lambda_3\lambda_4 | T | f0\lambda_3\lambda_4 \rangle \langle f\Omega\lambda_3\lambda_4 | B | i0\lambda_1\lambda_2 \rangle], \quad (2) \end{aligned}$$

where

$$\eta = (\eta')^2 (\lambda_3 - \lambda_4) e^{i(\lambda_1 - \lambda_2)\phi'},$$

$$\eta' = [e^{-i\phi'/2} \cos \frac{1}{2}\theta' \cos \frac{1}{2}\theta + e^{i\phi'/2} \sin \frac{1}{2}\theta' \sin \frac{1}{2}\theta] \cos \frac{1}{2}\theta'',$$

and

$$\cos \theta'' = \cos \theta \cos \theta' + \sin \theta \sin \theta' \cos \phi'.$$

We have discarded the product term containing two T -matrix elements because it represents the Feynman diagram where one elastic scatter takes place in the initial state and one takes place in the final state. We already neglected the diagrams, presumably of the same order of magnitude, where two elastic scatters take place in the initial (or final) state, and none take

place in the other state; therefore we must neglect the product term also.

The linear-momentum version of the absorption model, as expressed in Eq. (2), can be written as

$$A = \frac{1}{2}(S_f B + B S_i). \quad (3)$$

Comparison of Eq. (3) with Eq. (1) shows that the customary form of the absorption model modifies the Born amplitude by multiplication by the geometric mean of the initial- and final-state scattering S matrix, while Huff's version employs the arithmetic mean. This difference leads to some differences between our calculations and those of Ref. 5, to be discussed in Sec. V.

Given the helicity amplitudes of Eq. (2), it is straightforward to give the theoretical values for the $\{f_i\}$, defined in Sec. III, and the differential cross section. However, to give numerical values we need the coupling constants and the elastic cross-section behavior for $\Delta\omega$ scattering. We do not know the exact values for many of these parameters; we have therefore varied them in our application of the theory.

C. Coupling Constants

In this subsection we present what is known, either theoretically or experimentally, about the magnitudes of the coupling constants involved in the reaction $K^-p \rightarrow \Delta\omega$ proceeding via K and K^* exchange.

(1) $G(\omega K^+ K^-)$. From the decay of ϕ into $K^+ K^-$, we can determine the $G(\phi K^+ K^-)$ coupling constant by using

$$\Gamma_{\phi \rightarrow K^+ K^-} = \frac{2 G^2(\phi K^+ K^-)}{3} \frac{p^3}{4\pi m_\phi^2}.$$

Thus we have

$$\frac{G^2(\phi K^+ K^-)}{4\pi} = 1.2.$$

Then from $SU(3)$, where θ is the vector-meson mixing angle ($\theta = 40$ deg), we have

$$\frac{G^2(\omega K^+ K^-)}{4\pi} = \tan^2 \theta \frac{G^2(\phi K^+ K^-)}{4\pi} = 0.8.$$

Alternatively, using the $\rho \rightarrow \pi\pi$ decay, we find

$$\frac{G^2(\omega K^+ K^-)}{4\pi} = \frac{G^2(\rho\pi\pi)}{4\pi} \left(\frac{3}{4} \sin^2 \theta\right) \cong 0.7.$$

(2) $G(\bar{p}K^+\Lambda)$. Again we may use $SU(3)$ to relate $G(\bar{p}K^+\Lambda)$ to $G(\bar{p}\pi^0 p)$:

$$\frac{G^2(\bar{p}K^+\Lambda)}{4\pi} = \left(\frac{3-2\alpha}{\sqrt{3}}\right)^2 \frac{G^2(\bar{p}\pi^0 p)}{4\pi},$$

where $G^2(\bar{p}\pi^0 p)/4\pi = 14.6$, and α , the fraction of the interaction going through the d (symmetric) coupling,

is known to be $\simeq 0.75$.²² We find

$$G^2(\bar{p}K^+\Lambda)/4\pi \simeq 10.$$

(3) $G(\omega K^+K^{*-})$. Using the $\phi \rightarrow \rho\pi$ decay and the $\rho\pi$ model of the $\omega \rightarrow 3\pi$ decay, we may discover an approximate value for $G(\omega K^+K^{*-})$ through $SU(3)$. Let $\epsilon = G(\phi\pi^+\rho^-)/G(\omega\pi^+\rho^-)$. Then the allowed $SU(3)$ couplings lead to

$$\frac{G(\omega K^+K^{*-})}{G(\omega\pi^+\rho^-)} = 1 - \frac{3}{2}\sin^2\theta - \frac{3}{2}\epsilon\sin\theta\cos\theta.$$

Glashow and Socolow have predicted from their nonet coupling scheme that $\epsilon = -0.08$.²³ They have calculated a phase-space factor of 17 favoring $\phi \rightarrow \rho\pi$ over $\omega \rightarrow \rho\pi$; hence the determination of $\Gamma(\phi \rightarrow 3\pi) = 0.4 \pm 0.3$ MeV by Lindsey and Smith²⁴ leads to $|\epsilon| = 0.05 \pm 0.03$. We will use $\epsilon = -0.08$ to find $G(\omega K^+K^{*-})$. Thus we have

$$G(\omega K^+K^{*-})/G(\omega\pi^+\rho^-) = 0.64.$$

An expression for $G(\omega\pi^+\rho^-)$ in terms of the width of the ω has been derived by Gell-Mann, Sharp, and Wagner.²⁵ Their expression leads to

$$G^2(\omega\pi^+\rho^-)/4\pi \simeq 14;$$

therefore

$$G^2(\omega K^+K^{*-})/4\pi = 5.7.$$

(4) $G_V(\bar{p}K^{*+}\Lambda)$ and $G_T(\bar{p}K^{*+}\Lambda)$. The couplings of the ρ , ω , and ϕ vector mesons to the baryons can be deduced from nucleon-nucleon forces. However, in view of the wide variations in determinations, [e.g., Scotti and Wong²⁶ find $G_V^2(\bar{p}\omega p)/4\pi \simeq 3$; Bryan and Scott²⁷ find $G_V^2(\bar{p}\omega p)/4\pi \simeq 22$.] we probably should restrict ourselves to saying that $G_V^2/4\pi$ and $G_T^2/4\pi$ are ~ 10 .

Cabibbo²⁸ has suggested a scheme that predicts the ratio G_T/G_V . The interaction of baryons with vector particles can be written

$$\langle \bar{B} | V | B \rangle = \text{Tr}[\mathcal{O}V[\bar{B}, B] + \mathcal{E}V\{\bar{B}, B\}],$$

where V , \bar{B} , and B are matrices representing the vector-meson, antibaryon, and baryon octets, \mathcal{O} has the form $a\gamma_\mu + b\sigma_{\mu\nu}k_\nu$ and \mathcal{E} has the form $a'\gamma_\mu + b'\sigma_{\mu\nu}k_\nu$. If we assume that the electromagnetic current has the same transformation properties as the vector-meson octet, which is another way of saying that the photon and the vector mesons are all coupled to the same $SU(3)$ conserved currents, we can write the electromagnetic

²² A. W. Martin and K. C. Wali, Phys. Rev. **130**, 2455 (1963).

²³ S. L. Glashow and R. H. Socolow, Phys. Rev. Letters **15**, 329 (1965).

²⁴ J. S. Lindsey and G. A. Smith, Phys. Letters **20**, 93 (1966).

²⁵ M. Gell-Mann, D. Sharp, and W. G. Wagner, Phys. Rev. Letters **8**, 261 (1962).

²⁶ A. Scotti and D. Y. Wong, in *Proceedings of the Athens Topical Conference on Recently Discovered Resonant Particles, Athens, Ohio, April 1963* (University of Ohio, Athens, Ohio, 1963), p. 173.

²⁷ R. A. Bryan and B. L. Scott, Phys. Rev. **135**, B434 (1964).

²⁸ N. Cabibbo, lecture note, Lawrence Radiation Laboratory, 1964 (unpublished).

interaction of the proton and neutron as follows:

$$\langle \bar{p} | j_{e.m.} | p \rangle \sim \mathcal{E} - 3\mathcal{O}, \quad \langle \bar{n} | j_{e.m.} | n \rangle \sim -2\mathcal{E}.$$

But we know that

$$\langle \bar{p} | j_{e.m.} | p \rangle \sim \gamma_\mu + (\mu_p/2M)\sigma_{\mu\nu}k_\nu$$

and

$$\langle \bar{n} | j_{e.m.} | n \rangle \sim (\mu_n/2M)\sigma_{\mu\nu}k_\nu.$$

Hence we can solve for the forms of \mathcal{E} and \mathcal{O} :

$$\mathcal{E} = -\frac{1}{2}(\mu_n/2M)\sigma_{\mu\nu}k_\nu$$

$$\mathcal{O} = -\frac{1}{3}\gamma_\mu - \frac{1}{6}[(\mu_n + 2\mu_p)/2M]\sigma_{\mu\nu}k_\nu.$$

Now the $\bar{p}\Lambda K^*$ interaction is

$$\langle \bar{p} | j_{K^*} | \Lambda \rangle \sim 3\mathcal{O} - \mathcal{E} \sim \gamma_\mu + (\mu_p/2M)\sigma_{\mu\nu}k_\nu.$$

In our theory we have used the expression

$$\langle \bar{p} | j_{K^*} | \Lambda \rangle \sim G_V\gamma_\mu + [G_T/(m_2 + m_4)]\sigma_{\mu\nu}k_\nu.$$

Thus the prediction is

$$G_T/G_V \approx \mu_p = 1.79.$$

D. Relationship between $K^-p \rightarrow \Lambda\omega$ and $K^-p \rightarrow \Lambda\phi$

If the K and K^* exchange model is valid for $K^-p \rightarrow \Lambda\omega$, then we expect the same model to hold for $K^-p \rightarrow \Lambda\phi$, with coupling constants related through $SU(3)$. For example, we have

$$G(\omega K^+K^-)/G(\phi K^+K^-) = \tan\theta.$$

Also Glashow has pointed out that the ratio

$$R \equiv \left(\frac{G(\phi K^* \bar{K})}{G(\phi K \bar{K})} \right) \left(\frac{G(\omega K^* \bar{K})}{G(\omega K \bar{K})} \right)^{-1}$$

can be expressed as²⁹

$$R = -\tan\theta \left\{ \frac{\frac{3}{2}\sin\theta\cos\theta - \epsilon[1 - \frac{3}{2}\cos^2\theta]}{1 - \frac{3}{2}\sin^2\theta - \frac{3}{2}\epsilon\sin\theta\cos\theta} \right\}.$$

However, $\Lambda\phi$ elastic scattering in general is not determinable from $\Lambda\omega$ elastic scattering alone; the absorption parameters used for $\Lambda\phi$ in general would be different than those used for $\Lambda\omega$.

Lindsey has studied the reaction $K^-p \rightarrow \Lambda\phi$ in the same energy region as we have studied $K^-p \rightarrow \Lambda\omega$.³⁰ Some comments on the relationship of his results to ours are made in Sec. V.

V. APPLICATION OF THE ABSORPTION MODEL

A. Introduction

A computer program which puts Huff's treatment of the absorption model to practical use has been written

²⁹ Sheldon L. Glashow, Phys. Rev. Letters **11**, 48 (1963).

³⁰ James S. Lindsey, University of California Lawrence Radiation Laboratory Report No. UCRL-16526, 1965 (unpublished); see also Ref. 12.

at Lawrence Radiation Laboratory by J. Friedman (for the reaction $K^-p \rightarrow K^*p$) and modified by L. Hardy and S. Flatté (for $\pi^-p \rightarrow YK^*$ and $K^-p \rightarrow \Lambda\omega$).

In this section we first compare the results of our treatment with previously published results that used the angular-momentum treatment of the absorption model: We show that the different approximations that are used in the two treatments lead to qualitatively similar, though quantitatively somewhat different, predictions.

After satisfying ourselves that our method and our computer program are valid and useful within the context of the absorption model, we proceed to test the applicability of the absorption model to the reaction $K^-p \rightarrow \Lambda\omega$. We attempt to find confirmation of the idea, expressed in Sec. I, that t -channel exchange mechanisms do not become dominant until the highest momentum region, 2.6 BeV/c, the lower momenta being dominated by threshold and perhaps resonance effects.

The product of the coupling constants for K exchange which is found in the best solution at 2.6 BeV/c compares quite well with the $SU(3)$ prediction derived in Sec. IV. It then becomes of great interest to see if the $\Lambda\omega$ coupling constants, appropriately modified, can explain the characteristics of the reaction $K^-p \rightarrow \Lambda\phi$. We use some recently available data on $K^-p \rightarrow \Lambda\phi$ at 2.6 BeV/c to test the absorption model further, and we compare our results with the parameters obtained in $K^-p \rightarrow \Lambda\omega$.

B. Comparison with the Angular-Momentum Method

The two reactions similar to ours whose production characteristics have been explained by using the absorption model are $\pi^-p \rightarrow \rho^-p$ and $Kp \rightarrow K^*p$.⁵ Polarization information on the final fermion in these two reactions is not available; hence the only parameters that have been determined for these reactions are f_2 , f_3 , f_4 and the differential cross section. The parameters have usually been given in terms of a density-matrix notation³ for the final vector meson. The equations relating the two notations are

$$\rho_{00} = f_2, \quad \rho_{1,-1} = \frac{1}{2} - f_3 - \frac{1}{2}f_2$$

and

$$\text{Re}\rho_{10} = -f_4/2\sqrt{2}.$$

In the angular-momentum treatment, the absorption parameters are expressed in terms of the parameters C and γ where the absorption factor is

$$\exp(2i\delta) = 1 - C \exp(-\gamma J^2).$$

The correspondence with the total cross section, σ_T , and the slope of the elastic differential cross section, A , is

$$C = \sigma_T/4\pi A, \quad \gamma = 1/2q^2A.$$

If $\sigma_T(i)$, A_i and $\sigma_T(f)$, A_f are the parameters of initial-

and final-state scattering respectively, then we have

$$C_+ = \sigma_T(i)/4\pi A_i, \quad \gamma_+ = 1/2q^2A_i, \\ C_- = \sigma_T(f)/4\pi A_f, \quad \gamma_- = 1/2q^2A_f.$$

Figure 22(a) shows the predictions of the angular-momentum method taken from Jackson *et al.* for $\pi^-p \rightarrow \rho^-p$ at 4 BeV/c with π^0 exchange.⁵ The parameters they used are $C_+ = 0.76$, $\gamma_+ = 0.04$, $C_- = 1.0$, and $\gamma_- = 0.03$, which translate as $\sigma_T(i) = 28$ mb, $A_i = 7.5$ (BeV)⁻², $\sigma_T(f) = 56.7$ mb, and $A_f = 11.6$ (BeV)⁻². In Fig. 22(a) the squares are the results of our method; the agreement is excellent. This comparison checks only pseudoscalar exchange. To check vector exchange, we take the predictions given by Jackson *et al.* for the same reaction with some vector exchange added.⁵ The curves in Fig. 22(b) are the predictions of the angular-momentum treatment with the parameters ξ and η , given by Jackson *et al.* as

$$\xi = \frac{G(\pi^+V\rho^-)[G_V(\bar{p}Vp) + G_T(\bar{p}Vp)]}{2G(\pi^+\pi^0\rho^-)G(\bar{p}\pi^0p)}$$

and

$$\eta = \frac{G(\pi^+V\rho^-)G_T(\bar{p}Vp)}{G(\pi^+\pi^0\rho^-)G(\bar{p}\pi^0p)},$$

set at $\eta = 0$ and $\xi = \pm 0.25$ (lower curves) and $\xi = \pm 0.50$ (upper curves). Here R is the ratio of the results with nonzero ξ to the results for $\xi = 0$. We have determined that $\xi = \pm 0.25$ corresponds to $G_V = \pm 34$, $G_T = 0$ and that $\xi = \pm 0.50$ corresponds to $G_V = \pm 68$, $G_T = 0$. Our results are shown as squares (for positive G_V) and circles (for negative G_V). The agreement in ρ_{00} seems good, but the differential cross section appears to be in

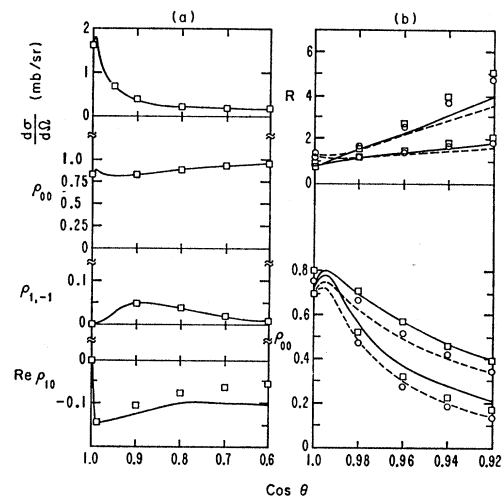


FIG. 22. Parameters predicted by the absorption model for the reaction $\pi^-p + \rho^-p$ at 4 GeV/c. The curves are taken from Jackson *et al.* (Ref. 5), and the points are from our method. (a) Pion exchange only; (b) some vector exchange added in the form of $\xi = \pm 0.25$ (lower solid and dashed curves and lower squares and circles) and $\xi = \pm 0.50$ (upper solid and dashed curves and upper squares and circles).

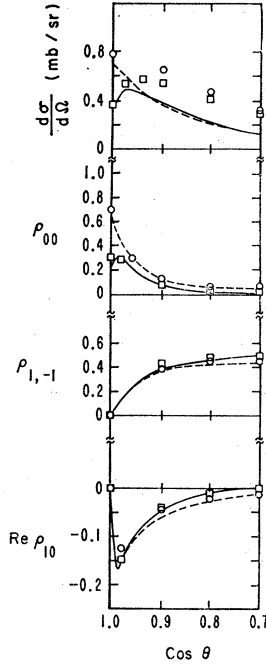


FIG. 23. Parameters predicted by the absorption model for the reaction $K^+p \rightarrow K^{*+}p$ at 3 GeV/c. The curves are taken from Jackson *et al.* (Ref. 5) and the points are from our method. The squares correspond to the solid lines and the circles to the dashed lines. See text for absorption parameters and coupling constants.

disagreement, our curves being higher than those of Jackson *et al.* To check further, we look at Fig. 23 which compares our results for $K^+p \rightarrow K^{*+}p$ at 3 GeV/c with those of Jackson *et al.* Again our agreement in the decay parameters is extremely satisfactory, but our differential cross-section curves lie higher than those of Jackson *et al.*

The comparisons show that for pion exchange, which involves many partial waves, Eq. (1) in the angular-momentum treatment and Eq. (3) in the linear-momentum representation yield very similar results. But for processes involving the exchange of a heavier vector meson, and so having fewer important partial waves, differences arise. The disagreements are caused mainly by the different method of absorption in Eqs. (2) and (3) as compared to Eq. (1). In Fig. 23 at $\cos\theta=0.7$, our value for the differential cross section is 0.3 mb and that of Ref. 5 is 0.12 mb. How much of a disagreement is this? We must remember that the crux of the calculation we are making is the calculation of how much the amplitude is absorbed. The unabsorbed cross section at this point is near 6 mb. Therefore we calculated the absorption as 95.0%, and Ref. 5 calculated 98.0%. In the amplitude this means we calculated 78%, and Ref. 5 used 86%; not such a large disagreement when considered in this way. We have discovered two important facts; our calculations and those of the angular-momentum treatment are acceptably close considering the completely different methods used, and the small differences between our answers result in large changes in the differential cross-section predictions. We can now explain why we agree in the forward direction: It is because the absorption is relatively small

there, and the calculated cross section is much less sensitive to differences in the absorption calculation. We can also explain why we agree on pseudoscalar exchange results—in fact we do not agree in the non-forward directions, but both our results are so small compared to the forward peak that a large percentage difference goes unnoticed.

We now say the following: the two different treatments of the absorption model agree closely on the effect of pseudoscalar exchange, but disagree by large factors (in two cases, by 2 or 3) on the effect of vector exchange in the differential cross section. The decay correlations are not very sensitive to the difference in the two methods. The differences in the cross section will be buried in the variation of vector coupling constants which are not known. In other words the vector couplings found in Ref. 5 would need to be reduced by a factor ~ 2 , if used in our treatment. We do not believe that either answer is inherently right; the results are too sensitive to the calculational technique. However, it seems reasonable that the results of one program will be internally consistent, and therefore the ratios of vector couplings determined by one program will have an approximate meaning.

C. Comparison with Experiment for $K^-p \rightarrow \Lambda \omega$

To predict an experimental result, we must provide the theory with the following parameters:

$$\begin{aligned}
 g_p^2 &= G^2(K^-K^+\omega)G^2(\bar{p}K^+\Lambda)/(4\pi)^2 && = K\text{-meson-exchange coupling;} \\
 g_V &= G(K^-K^*\omega)G_V(\bar{p}K^*\Lambda) && = K^*\text{-exchange vector coupling;} \\
 g_T &= G(K^-K^*\omega)G_T(\bar{p}K^*\Lambda) && = K^*\text{ exchange tensor coupling;} \\
 \sigma_T(i)\{\sigma_T(f)\} &= K^-p\{\Lambda\omega\} && \text{total cross section;} \\
 A_i\{A_f\} &= K^-p\{\Lambda\omega\} && \text{elastic differential cross-section slope} \\
 &&& \text{in the forward direction;} \\
 \psi &= \text{possible nonzero phase of the transition matrix} \\
 &&& \text{element for elastic scattering.}
 \end{aligned}$$

One of the predictions arising from these parameters is the differential cross section for $K^-p \rightarrow \Lambda\omega$. Since the data give cross sections for $K^-p \rightarrow \Lambda\omega \rightarrow \Lambda\pi^+\pi^-\pi^0$ we have multiplied all experimental cross sections by 1.1 to account for other ω decay modes.

An important comment which we must make immediately is that *if we assume ψ is zero, then the theory will predict that f_5 through f_{12} are identically zero everywhere.* The data at the highest energy are actually not too inconsistent with this prediction; however a nonzero ψ does significantly improve the fits obtained. In all our fits we have assumed that the ψ for K^-p elastic scattering is the same as the ψ for $\Lambda\omega$ elastic scattering, and that ψ is not a function of production angle. These are drastic approximations, but the effect of ψ is only felt significantly by f_5 through f_{12} , which are not very well determined anyway. We note that the values of ψ for

TABLE IX. Best-fit parameters for $K^-p \rightarrow \Lambda\omega$.

Momentum (BeV/c)	Theory ^a	No. of data points	χ^2	$\sigma_T(f)$ (mb)	A_f (BeV) ⁻²	ψ	g_p^2	g_V	g_T
1.5	K	26	144	45.0	4.7	0.47	10.4	0	0
1.5	$KK^*(1)$	26	140	9.1	-6.0	-0.54	3.0	-24.6	-6.2
1.5	$KK^*(2)$	26	54	41.9	1.7	0.36	16.6	36.7	22.1
1.7	K	26	71	61.9	9.8	0.51	12.7	0	0
1.7	$KK^*(1)$	26	70	57.0	19.5	0.02	12.2	-28.2	-5.8
1.7	$KK^*(2)$	26	49	60.8	10.5	0.43	14.9	20.5	10.1
2.1	K	26	302	0	0	-0.14	2.9	0	0
2.1	$KK^*(1)$	26	66	0	0	-0.06	0.5	-11.8	-9.9
2.1	$KK^*(2)$	26	76	0	0	-0.20	0.7	10.9	10.1
2.6	K	36	167	83.1	13.8	0.16	16.2	0	0
2.6	$KK^*(1)$	36	68	83.0	14.2	-0.10	7.4	-28.9	-8.8
2.6	$KK^*(2)$	36	83	83.2	13.7	0.12	11.8	25.6	3.4
2.6	$KK^*(K^-p \rightarrow \Lambda\phi)$	28	78	81.6	13.1	0.07	6.9	32.0	20.3

^a K means K exchange only. $KK^*(1)$ means K and K^* exchange with the relative sign between the K^* and K couplings negative; $KK^*(2)$ means the sign is positive.

the best fits at 2.6 BeV/c are small, in keeping with our belief that ψ is close to zero in the very forward direction.

We have set $\sigma_T(i)=30$ mb and $A_i=7.5$ (BeV)⁻² everywhere. This is certainly a good approximation in the case of $\sigma_T(i)$; Lynch³¹ has shown us preliminary data from 1.5 to 2.6 BeV/c in which A_i varied from 7.0 to 8.5 (BeV)⁻². Any deviation from 7.5 (BeV)⁻² can easily be taken into account by a small variation in the final-state absorption parameters $\sigma_T(f)$ and A_f .

At each momentum we have tried two different fits. First, we have tried K exchange only, varying g_p^2 , $\sigma_T(f)$, A_f , and ψ . Then we have included K^* exchange, adding g_V and g_T as parameters. Jackson *et al.*⁵ have

already observed that two regions of vector-meson exchange couplings often give comparably good fits to the data; one corresponds to constructive and the other to destructive interference between the vector exchange and the pseudoscalar exchange. We find similar results, and we have tabulated both fits where necessary.

The parameters and χ^2 for the best fits are given in Table IX, and the curves corresponding to the fits at 2.6 and 1.7 BeV/c are shown in Figs. 24 and 25. It is difficult to state errors on the parameters at 2.6 BeV/c, because the curves are in qualitative but clearly not quantitative agreement with the data. This also results in χ^2 which are certainly higher than would be accept-

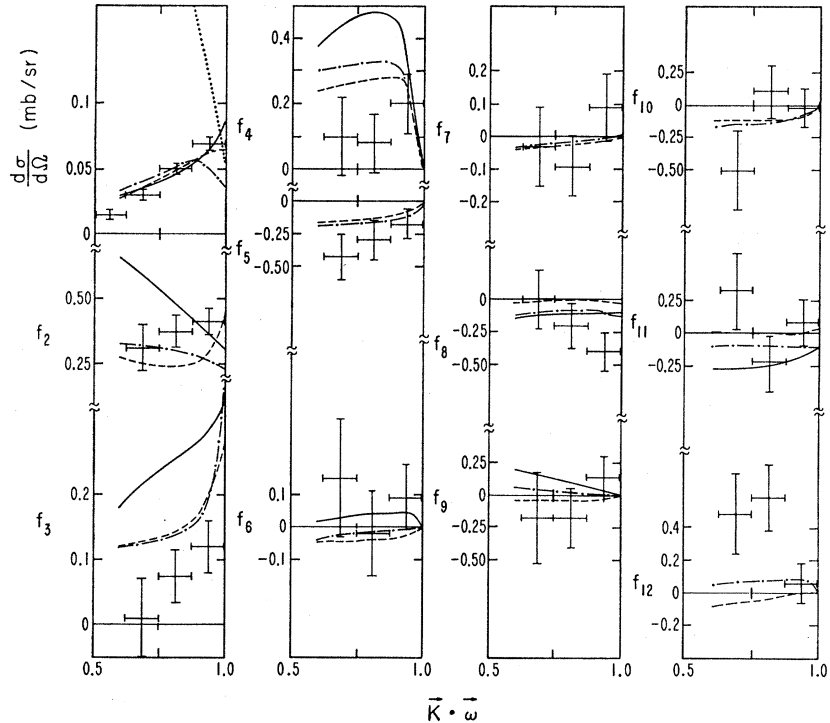


FIG. 24. Data at forward production angles for 2.6-BeV/c $K^-p \rightarrow \Lambda\omega$ events. The solid curves correspond to the best fits for K exchange only, the dashed curves to $KK^*(1)$ best fit, the dash-dot curve to $KK^*(2)$ best fit, and the dotted curve to K exchange only with no absorption and a K coupling equal to that used in the solid curves.

³¹ G. Lynch, Lawrence Radiation Laboratory, Berkeley, California (private communication).

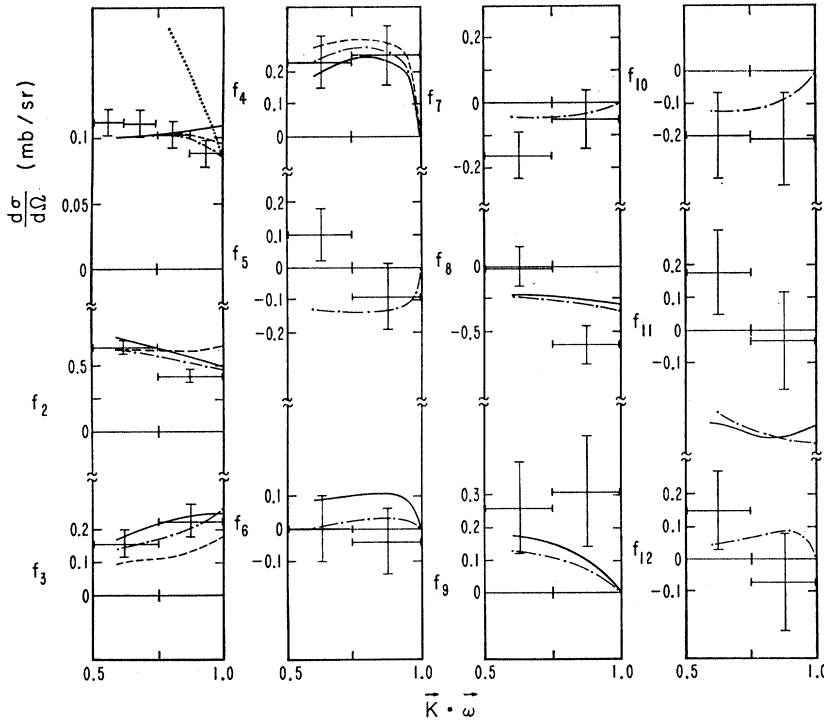


FIG. 25. Data at forward production angles for 1.7 BeV/c $K^-p \rightarrow \Lambda\omega$ events. The solid curves correspond to the best fits for K exchange only, the dashed curves to $KK^*(1)$ best fit, the dash-dot curve to $KK^*(2)$ best fit, and the dotted curve to K exchange only with no absorption and a K coupling equal to that used in the solid curves.

able for a perfect theory; one must judge by the curves whether one agrees that “qualitative agreement” has been reached. We prefer to show the curves for the best fits and state that changes of the order of 20% in the coupling constants would definitely give much worse fits. At the lower momenta, errors would not be meaningful, since we wish to argue that the theory is not applicable.

Some comments on the fits at each momentum are made below.

1. 2.6 BeV/c

First we note that $C_- \equiv \sigma_T(f)/4\pi A_f$ is 1.2. To be consistent with our assumption that the elastic scattering is almost entirely the shadow of the inelastic processes, C should be ≤ 1 . However, since so far $C_- = 1$ has given the best results in the absorption model, and since we have in no way constrained our parameters to satisfy $C \leq 1$, we feel that a value of 1.2 is quite reasonable and acceptable. In fact, since our formalism essentially averages the initial- and final-state S -matrix elements, and since we fixed our initial-state $C_+ = \sigma_T(i)/4\pi A_i$ at 0.8, then $C_- = 1.2$ corresponds to total absorption of the s wave, a prominent feature of other successful absorption-model fits.

The total cross section for $\Lambda\omega$ scattering of ~ 80 mb may be compared with estimates of ~ 80 mb for $\sigma_T(\rho N)$ made by Drell and Trefil.³²

³² S. D. Drell and J. S. Trefil, Phys. Rev. Letters **16**, 552 (1966); **16**, 832 (E) (1966). In the Erratum they estimate $66 \text{ mb} < \sigma(\rho_0 N) < 94 \text{ mb}$ at a ρ momentum of 4.4 BeV/c.

Next we note that the K -exchange coupling,

$$g_p^2 = G^2(K-K^+\omega)G^2(\bar{p}K^+\Lambda)/(4\pi)^2,$$

for the best fit is 7.4, in remarkable agreement with the $SU(3)$ prediction derived in Sec. IV, $g_p^2 \cong 7$ to 8. The K^* -exchange couplings are certainly of a reasonable magnitude.

The curves show a qualitative agreement with the data; the differential-cross-section fit is excellent. The worst quantitative discrepancies occur in f_3 and f_{12} , but even in f_3 the shape is similar. On the whole, the absorption model appears to give a reasonable qualitative picture at 2.6 BeV/c.

2. 2.1 BeV/c

We find $\chi^2 = 177$ if we use the parameters determined at 2.6 BeV/c. If the final-state absorption parameters are allowed to vary freely, A_f goes negative and $\sigma_T(f)$ becomes small (< 5 mb), a reflection of the lack of forward peaking in the differential cross section. We therefore set $\sigma_T(f) = 0$ for our final fits. We then find that g_p^2 is at least an order of magnitude below what we expect. (The two fits with K^* exchange really correspond to more or less the same region. One may think of it as positive g_V and g_T with small g_p ; in one case g_p is negative and small, in the other positive and small.)

Thus at 2.1 BeV/c, we find two very unpleasant facts, if we want to believe the absorption model. First, the $\Lambda\omega$ total cross section is extremely small, in contradiction to estimates of the ρN total cross sections (~ 80 mb at

4 BeV/c ρ laboratory momentum) made by Drell and Trefil,³² and to other absorption model fits such as $p\rho^-$ and pK^* . Second, the K -exchange coupling is an order of magnitude smaller than one expects.

3. 1.7 BeV/c

The fits at 1.7 BeV/c are quite reasonable in all respects. For the final state, we have $C=0.6$ for the best fit and $g_p^2=12$. Since we do not expect the absorption model to apply here, the only comment to make, obviously, is that a theory is not required to fail where it is inapplicable, only to succeed where it is applicable. We find $\chi^2=196$ if we use the parameters determined at 2.6 BeV/c.

4. 1.5 BeV/c

Here the model again has trouble. The best-fit value of C is 5.2, which is clearly unacceptable. Essentially A_f tends to be much too small. Also ψ is becoming rather large. Of course when C is this large, our approximation that $(1-T)^{1/2} \cong 1 - \frac{1}{2}T$ is no longer even approximately good. We can say that the 1.5-BeV/c data are not well explained when treated by our method for the absorption model. We find $\chi^2=326$ if we use the parameters determined at 2.6 BeV/c.

D. Comparison with Experiment for $K^-p \rightarrow \Lambda\phi$

The fact that g_p^2 , the K -exchange coupling, came out quite reasonable for $K^-p \rightarrow \Lambda\omega$ at 2.6 BeV/c is gratifying. It then becomes of great interest whether the characteristics of $K^-p \rightarrow \Lambda\phi$ are consistent with these couplings also. We have translated the results of Lindsey³⁰ on $K^-p \rightarrow \Lambda\phi$ at 2.6 BeV/c into our notation and plotted the results in Fig. 26. The solid curve is calculated from the parameters determined at 2.6 BeV/c for $K^-p \rightarrow \Lambda\omega$, appropriately modified. The modifications, given in Sec. IV, are

$$g_p(\Lambda\phi) = g_p(\Lambda\omega) \cot\theta_m = 1.19g_p(\Lambda\omega)$$

and

$$g_V \text{ or } \tau(\Lambda\phi) = g_V \text{ or } \tau(\Lambda\omega) [-R \cot\theta_m] = -1.7g_V \text{ or } \tau(\Lambda\omega).$$

The χ^2 for the solid curve is 552 for 28 data points, where we have assumed that the error matrix for the decay parameters is diagonal. This is not a bad assumption.³⁰

We then allowed all parameters to vary and found as the best fit the dashed curve in Fig. 26. The χ^2 is 77.8. The parameters of the dashed curve are $\sigma_T(f) = 81.6$ mb, $A_f = 13.1$ (BeV)⁻², $\psi = 0.07$, $g_p^2 = 6.9$, g_V

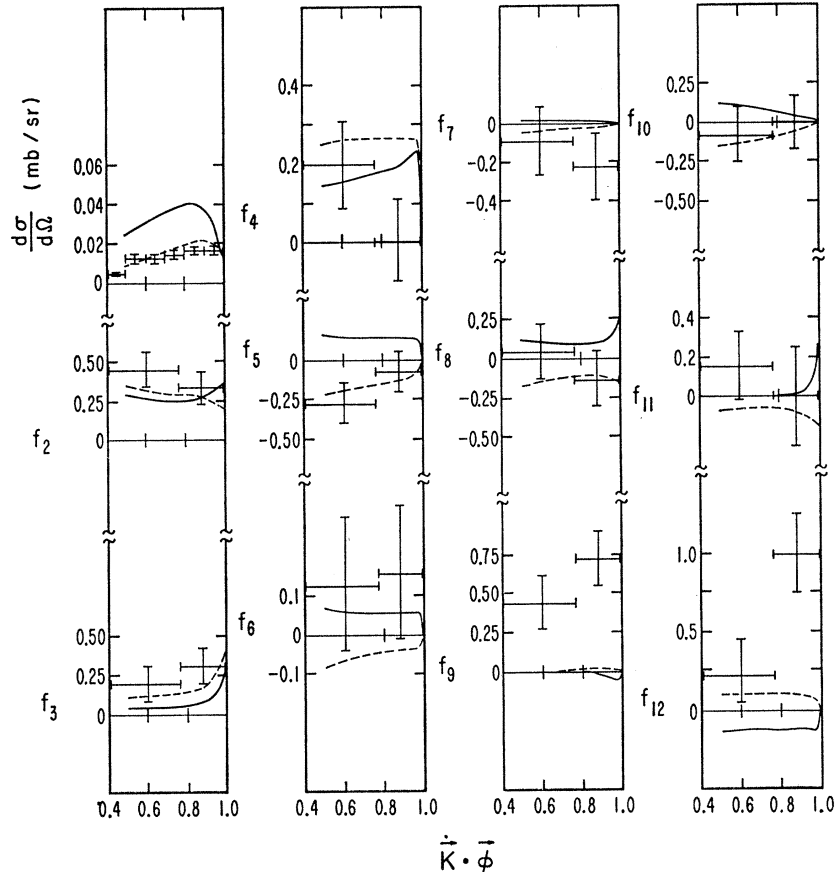


FIG. 26. Data taken from Lindsey (Ref. 30) for the reaction $K^-p \rightarrow \Lambda\phi$ at 2.6 BeV/c. The solid curves are the predictions of the absorption model with absorption parameters identical to those determined by the $KK^*(1)$ solution to $\Lambda\omega$ at 2.6 BeV/c and with coupling constant obtained from the $\Lambda\omega$ fit by invoking exact $SU(3)$. The dashed curves correspond to the best fit with a free variation of parameters. See text for a comparison of couplings determined in the best fits.

= 32.0, and $g_T = 20.3$. Hence we have

$$\frac{G(K^-K^+\phi)}{G(K^-K^+\omega)} \cong \left(\frac{6.9}{7.4}\right)^{1/2} = 1.0$$

where we expect 1.2,

$$\frac{G_V(K^-K^*\phi)}{G_V(K^-K^*\omega)} \cong \frac{32.0}{-28.9} = -1.1$$

where we expect -1.7, and

$$\frac{G_T(K^-K^*\phi)}{G_T(K^-K^*\omega)} \cong \frac{20.3}{-8.8} = -2.3$$

where we expect -1.7. Of course we have chosen the fit to $\Lambda\omega$ which best meets the predictions. (It is also the best fit.)

Glashow²⁹ has pointed out that the test that is least sensitive to kinematical effects is the ratio R . We find using G_V that

$$R = \left(\frac{32.0}{\sqrt{6.9}}\right) \left(\frac{\sqrt{7.4}}{-28.9}\right) = -1.1,$$

where we expect -1.4, and using G_T we find

$$R = \left(\frac{20.3}{\sqrt{6.9}}\right) \left(\frac{\sqrt{7.4}}{-8.8}\right) = -2.4,$$

where we expect -1.4.

Cabibbo's prediction (see Sec. IV) that $G_T/G_V = 1.79$ is not verified since G_T in our best fits is about a factor of 2 smaller than G_V . Cabibbo's scheme also predicts G_T/G_V for the $\bar{p}p\rho^0$ vertex as $\mu_p - \mu_n = 4.7$. Using the

reaction $K^+p \rightarrow K^*p$, Jackson *et al.*⁵ found $G_T/G_V(\bar{p}p\rho^0) \leq 1$, again not in agreement with the prediction.

Since the vector-meson exchange formalism is in much doubt, the vector-coupling comparisons may be academic; however, we have avoided the main problem of vector exchange—its energy dependence—by working always at the same energy (although not at the same distance from threshold).

The orders of magnitude seem to be clearly in order, and even the signs seem of some significance. (The signs are relative ones between g_p and either g_V or g_T .)

E. Conclusions

We have shown that the characteristics of the reactions $K^-p \rightarrow \Lambda\omega$ and $K^-p \rightarrow \Lambda\phi$ at 2.6 BeV/c at forward production angles are explained reasonably well by the absorption model with K and K^* exchange. The couplings obtained from best fits to the data are in remarkable qualitative agreement with the predictions of $SU(3)$.

The qualitative features of the reaction $K^-p \rightarrow \Lambda\omega$ at lower momenta (namely the lack of a strong forward peak) indicate that t -channel exchanges are not dominant; therefore we would not expect the absorption model to work. If it did work we could not fault the model, but a theory which works everywhere, regardless of whether it is applicable or not, is not a very testable theory. We find at 1.5 and 2.1 BeV/c the absorption model does fail to explain the data, while at 1.7 BeV/c it works.

ACKNOWLEDGMENTS

I thank Professor M. Lynn Stevenson and Professor Luis W. Alvarez for their continued support, encouragement, and guidance. I also thank Jerome Friedman, Dr. Ronald Ross, and Dr. Robert Huff for their many discussions on the absorption model.